Available online at www.sciencedirect.com

SciVerse ScienceDirect

Geochimica et Cosmochimica Acta 117 (2013) 33–52

Geochimica et Cosmochimica Acta

www.elsevier.com/locate/gca

Dissolved strontium in the subterranean estuary – Implications for the marine strontium isotope budget

Aaron J. Beck [a,*], Matthew A. Charette [b], J. Kirk Cochran [c], Meagan E. Gonneea [b], Bernhard Peucker-Ehrenbrink [b]

[a] Virginia Institute of Marine Science, College of William & Mary, P.O. Box 1346, Gloucester Point, VA 23062, USA
[b] Department of Marine Chemistry and Geochemistry, Woods Hole Oceanographic Institution, Woods Hole, MA 02543, USA
[c] School of Marine and Atmospheric Sciences, Stony Brook University, Stony Brook, NY 11794, USA

Received 18 April 2012; accepted in revised form 17 March 2013; available online 30 March 2013

Abstract

Submarine groundwater discharge (SGD) to the ocean supplies Sr with less radiogenic $^{87}Sr/^{86}Sr$ than seawater, and thus constitutes an important term in the Sr isotope budget of the modern ocean. However, few data exist for Sr in coastal groundwater or in the geochemically dynamic subterranean estuary (STE). We examined Sr concentrations and isotope ratios from nine globally-distributed coastal sites and characterized the behavior of Sr in the STE. Dissolved Sr generally mixed conservatively in the STE, although large differences were observed in the meteoric groundwater end-member Sr concentrations among sites (0.1–24 μM Sr). Strontium isotope exchange was observed in the STE at five of the sites studied, and invariably favored the meteoric groundwater end-member signature. Most of the observed isotope exchange occurred in the salinity range 5–15, and reached up to 40% exchange at salinity 10. Differences in fresh groundwater Sr concentrations and isotope ratios ($^{87}Sr/^{86}Sr = 0.707–0.710$) reflected aquifer lithology. The SGD end-member $^{87}Sr/^{86}Sr$ must be lower than modern seawater (i.e., less than 0.70916) in part because groundwater Sr concentrations are orders of magnitude higher in less-radiogenic carbonate and volcanic island aquifers. A simple lithological model and groundwater Sr data compiled from the literature were used to estimate a global average groundwater end-member of 2.9 μM Sr with $^{87}Sr/^{86}Sr = 0.7089$. This represents a meteoric-SGD-driven Sr input to the ocean of $0.7–2.8 \times 10^{10}$ mol Sr y^{-1}. Meteoric SGD therefore accounts for 2–8% of the oceanic Sr isotope budget, comparable to other known source terms, but is insufficient to balance the remainder of the budget. Using reported estimates for brackish SGD, the estimated volume discharge at salinity 10 ($7–11 \times 10^{15}$ L y^{-1}) was used to evaluate the impact of isotope exchange in the STE on the brackish SGD Sr flux. A moderate estimate of 25% isotope exchange in the STE gives an SGD Sr end-member $^{87}Sr/^{86}Sr$ of 0.7091. The brackish SGD Sr flux thus accounts for 11–23% of the marine Sr isotope budget, but does not appear sufficient to balance the ~40% remaining after other known sources are included. Substantial uncertainties remain for estimating the SGD source of Sr to the global ocean, especially in the determination of the volume flux of meteoric SGD, and in the paucity of measurements of groundwater Sr isotope composition in major SGD regions such as Papua New Guinea, the South America west coast, and West Africa. Consequently, our global estimate should be viewed with some caution. Nevertheless, we show that the combined sources of meteoric SGD and brackish SGD coupled with isotope exchange in the STE may constitute a substantial component (~13–30%) of the modern oceanic $^{87}Sr/^{86}Sr$ budget, likely exceeding less radiogenic Sr inputs by sedimentary diagenesis and hydrothermal circulation through the mid-ocean ridge system. Temporal variation in SGD Sr fluxes and isotope composition may have contributed to fluctuations in the oceanic $^{87}Sr/^{86}Sr$ ratio over geologic time.

* Corresponding author. Tel.: +1 804 684 7494; fax: +1 804 684 7786.
E-mail address: abeck@vims.edu (A.J. Beck).

0016-7037/$ - see front matter © 2013 Elsevier Ltd. All rights reserved.
http://dx.doi.org/10.1016/j.gca.2013.03.021

1. INTRODUCTION

The Sr isotope composition of the world's oceans may not be at steady state, as suggested by the well-documented increase of $^{87}Sr/^{86}Sr$ ratios from 0.7077 approximately 40 million years before present, to the current seawater value of 0.70916 (Hess et al., 1986; Veizer, 1989; Hodell et al., 1991; Paytan et al., 1993; Henderson et al., 1994; Farrell et al., 1995), as well as the apparent imbalance in the $^{88}Sr/^{86}Sr$ budget of the modern ocean (Krabbenhöft et al., 2010). However, data from the most recent ~500 ky indicate that the rate of change of the oceanic $^{87}Sr/^{86}Sr$ ratio has slowed considerably or ceased (Capo and DePaolo, 1990; Henderson et al., 1994; Farrell et al., 1995). Strontium isotope budgets in the ocean (Palmer and Edmond, 1989) have typically included input terms for rivers, diffusive diagenetic flux from sediments, and hydrothermal circulation. Previous estimates of the supply of less radiogenic Sr from hydrothermal circulation through the mid-ocean ridge system were sufficient to balance the Sr isotope budget (Palmer and Edmond, 1989). However, Chaudhuri and Clauer (1986) proposed that the discharge of groundwater to the subsurface ocean, which they envisioned as fresh submarine groundwater discharge (SGD) and termed "run-out", could supply less radiogenic Sr to the oceans and that this term also should be included in the Sr isotope budget. Recent work by Allègre and coworkers (2010) supports the idea that the oceanic $^{87}Sr/^{86}Sr$ budget may be missing critical components such as island arc and ocean island weathering, and they argue that subsurface water discharges can balance the $^{87}Sr/^{86}Sr$ budget. In order to properly interpret past variations in seawater Sr isotope ratios, a better understanding of the modern oceanic Sr isotope budget is required.

The $^{87}Sr/^{86}Sr$ ratio of seawater increases due to fluvial transport of radiogenic Sr weathered from crustal rocks (Palmer and Edmond, 1992), including radiogenic runoff from the Himalaya/Tibetan Plateau region drained by the Ganges–Brahmaputra river system (Edmond, 1992; Palmer and Edmond, 1992; Krishnaswami et al., 1992). While this contribution is currently among the most radiogenic large sources of dissolved Sr to seawater, new evidence from soil carbonates in the Ganges–Brahmaputra drainage basin suggests that the highly radiogenic Sr composition of these waters might be caused by changes in land-use that enhanced weathering and erosion in the Lesser Himalayan region in historic times (Rahaman et al., 2011). The input of radiogenic Sr from rivers is offset by less radiogenic Sr sources such as diagenetic and hydrothermal modification of submarine basalts (Albarede et al., 1981) and seafloor sediments (Elderfield and Gieskes, 1982), as well as subaerial weathering of marine carbonates (Starinsky et al., 1980; Palmer and Edmond, 1992).

Recent work in the Bengal Basin has indicated that direct discharge of groundwater to the ocean may be an important source term in the global Sr budget of seawater and may play a role in determining the marine $^{87}Sr/^{86}Sr$ composition (Basu et al., 2001; Dowling et al., 2003). Allègre et al. (2010) concluded that subsurface water flux (i.e., SGD) from volcanic islands can supply the required less-radiogenic Sr ($^{87}Sr/^{86}Sr = 0.7035$) to balance the marine Sr isotope budget. However, SGD from the Bengal Basin has a very different, highly radiogenic $^{87}Sr/^{86}Sr$ signature (~0.72; Basu et al., 2001). It is clear from these disparate sources that there is not a single, common SGD end-member, and that the isotopic composition of global SGD-driven Sr input is a combination of many different groundwater types. On balance, global-average SGD-derived Sr input to the ocean may not have an $^{87}Sr/^{86}Sr$ composition much different from modern seawater.

SGD has gained increasing attention since the landmark work of Moore (1996) showed that SGD comprising a combination of meteoric and saline components can drive a chemical flux in great excess of the meteoric groundwater discharge alone. Biogeochemical reactions such as ion exchange, dissolution and precipitation, and metal redox cycling occur in the mixing zone between meteoric and saline groundwaters (the so-called "subterranean estuary", or STE; Moore, 1999), resulting in a brackish SGD end-member that is very different in composition from either of its end-members (Shaw et al., 1998; Charette and Sholkovitz, 2006). Given a sufficient degree of enrichment for a particular constituent, SGD can represent a significant chemical flux, even on oceanic scales, as has been argued for Nd (Johannesson and Burdige, 2007; Johannesson et al., 2011), Fe (Windom et al., 2006), and Ra (Moore et al., 2008; Moore, 2010). The demonstration of large SGD-driven fluxes of Ba and Ra in the Bengal Basin (Moore, 1997) spurred studies identifying a substantial Sr flux in that region (Basu et al., 2001; Dowling et al., 2003). A key underlying assumption to these studies was that the groundwater Sr end-member is not chemically modified during passage through the subterranean estuary. However, emerging evidence suggests that major elements such as Ca and Sr and their isotopes may mix non-conservatively in the dynamic STE mixing zone (Holmden et al., 2012; Rahaman and Singh, 2012), highlighting the importance of this interface to SGD-driven chemical flux.

The purpose of this contribution is to perform a more comprehensive assessment of the potential SGD-driven Sr flux by examining dissolved Sr in groundwater from a variety of coastal aquifer types, and by characterizing Sr behavior in the STE. $^{87}Sr/^{86}Sr$ ratios are examined to determine the potential importance of subterranean estuary processes in regulating the $^{87}Sr/^{86}Sr$ composition of the SGD-driven Sr flux. We demonstrate that submarine groundwater discharge (both fresh and brackish) is a major source of Sr to the modern ocean with a $^{87}Sr/^{86}Sr$ slightly less radiogenic than present-day seawater, and we present a revised oceanic $^{87}Sr/^{86}Sr$ budget that includes the groundwater component.

2. METHODS

2.1. Sample collection and analysis

Samples for Sr analysis were collected from a wide variety of sites (Fig. 1), and from both surface water and groundwater (Table 1). Brackish groundwater was collected either from wells, or from the subterranean estuary using push-point piezometers (Charette and Allen, 2006; Charette

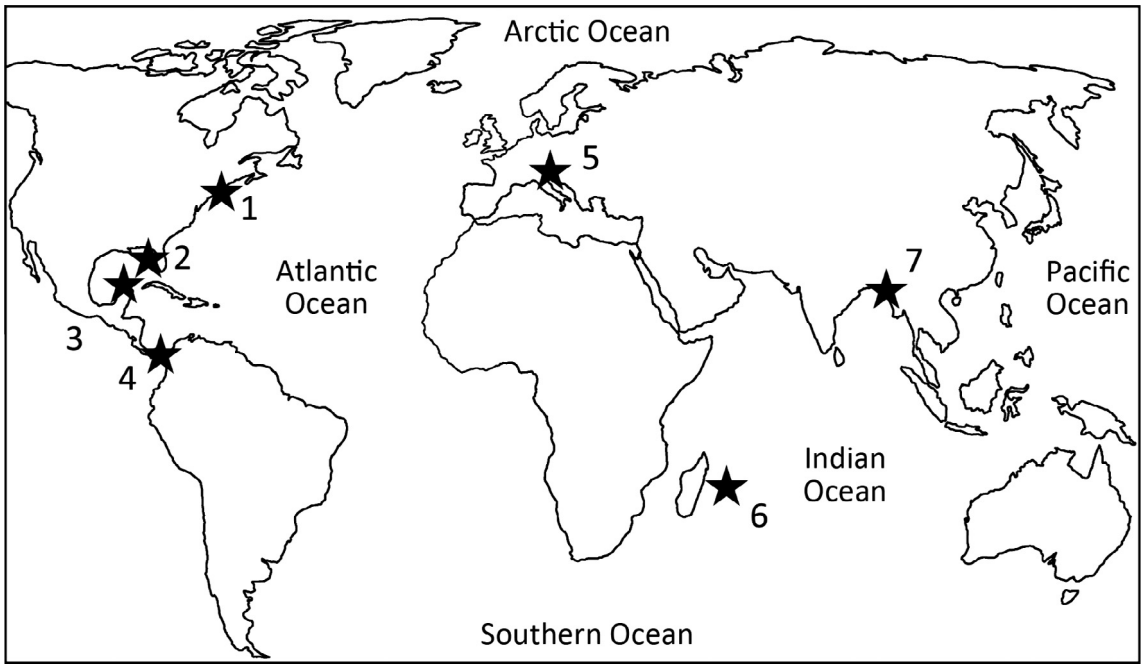

Fig. 1. Sample locations. (1) Massachusetts (Waquoit Bay, Pamet River) and New York (Great South Bay), USA; (2) Florida, USA; (3) Yucatan, Mexico; (4) Panama; (5) Venice, Italy; (6) Mauritius; (7) Bangladesh.

Table 1
Sample sites, collection dates, and site information.

Site	Date sampled	Sample types	Aquifer type	Associated reference
Bay of Bengal, Bangladesh	January–February 1987	River, Ocean	Ganges–Brahmaputa*, igneous granites and gneisses	Alam et al. (2003), Krishnaswami et al. (1992), Moore (1997) and Carroll et al. (1993)
Great South Bay, NY, USA	August 2006	STE, River, Ocean	Granitic glacial till	Beck et al. (2010) and Xin (1993)
Pamet River, MA, USA	July 2005	STE, Ocean	Granitic glacial till	Bau et al. (2004) and Charette (2007)
Waquoit Bay, MA, USA	June 2006	STE, Ocean	Granitic glacial till	Charette and Sholkovitz (2006), Bau et al. (2004), Cambareri and Eichner (1998) and Mulligan and Charette (2006)
Manatee R. basin, Florida, USA	February 2007	STE, Ocean	Carbonate	Hickey et al. (2010)
Flic-en-Flac Lagoon, Mauritius	March 2005	STE, Ocean	Basalt	Burnett et al. (2006) and Nohda et al. (2005)
Veraguas Province, Panama	December 2004	STE, Ocean	Quartz diorites, granodiorites, basaltic andesites (island arc)	Coates et al. (2004)
Celestún Lagoon, Yucatan, Mexico	May 2007	Cenote, STE, Ocean	Carbonate, Evaporite	Charette et al. (2008), Perry et al. (2002, 2009) and Young et al. (2008)
Venice Lagoon, Italy	November 2005	STE, River, Ocean	Carbonate	Garcia-Solsona et al. (2008), Brambati et al. (2003) and Rapaglia et al. (2010)

* See text.

and Sholkovitz, 2006) or multi-level samplers (Beck, 2007). Groundwater from a sinkhole (cenote) on the Yucatan Peninsula (Mexico) was sampled with a Niskin bottle. Samples were filtered (0.2 or 0.45 μm) and acidified to pH < 2 with HNO_3 or HCl. Samples were collected by different researchers using slightly different methods over approximately

15 years, but these minor differences are not expected to affect the data reported here.

Strontium concentration was determined by isotope dilution. Briefly, 0.1 to 2 mL of sample and a corresponding amount of ^{84}Sr tracer were mixed and dried in Teflon beakers, oxidized with between one and three 100 μL aliquots of concentrated HNO_3, and reconstituted in 2 mL of 6 N HNO_3. Mini-columns (4 cm length, free column volume (FCV): 200 μL) were slurry packed with acid-washed Sr-Spec resin (Eichrom® LLC; Horwitz et al., 1991; Pin and Bassin, 1992; Pin et al., 1994) in MilliQ water. The resin was rinsed with three FCVs of MilliQ water, and pre-conditioned with three FCVs of 6 N HNO_3. The sample was then passed through the resin under slight vacuum, and the evaporation beaker and loaded resin were rinsed three times with 1 mL 6 N HNO_3. Strontium was then eluted from the columns using six 500 μL aliquots of MilliQ water. The procedural Sr blank was 88 ± 38 pg (average ± 1 s.d.), less than 1% of the lowest sample. Isotope ratios needed for the isotope dilution calculations were determined on a ThermoFisher Element2 ICPMS by monitoring the ^{84}Sr and ^{88}Sr peaks. Strontium-84 counts were corrected for ^{84}Kr interferences (inherent in the Ar carrier gas) by monitoring ^{82}Kr. Final Sr concentration values had better than 3% precision based on repeated extraction and analysis of replicate samples.

The same method was employed for $^{87}Sr/^{86}Sr$ analysis using 1–5 mL of unspiked sample (depending on Sr concentration). After purification, samples were diluted to a concentration of approximately 200 ng g^{-1} Sr, and Sr isotope ratios were measured on a ThermoFisher Neptune multi-collector ICPMS by monitoring ^{82}Kr, ^{83}Kr, ^{84}Sr, ^{85}Rb, ^{86}Sr, ^{87}Sr and ^{88}Sr. The $^{86/88}Sr$ was normalized to the accepted value of 0.1194 to correct for instrument mass bias, which was further applied to $^{83/84}Kr$, $^{83/86}Kr$, $^{85/87}Rb$, $^{84}Sr/^{86}Sr$, $^{84}Sr/^{88}Sr$ and $^{87}Sr/^{86}Sr$ using the exponential law. These mass bias-corrected ratios were used to correct for Kr interferences on ^{84}Sr (~5% of mass 84) and ^{86}Sr (~0.1% mass 86) and Rb interferences on ^{87}Sr (<0.01% of mass 87) following the methodology of Jackson and Hart (2006). Analysis of standard reference material NBS 987 gave an $^{87}Sr/^{86}Sr$ value of 0.710240 ± 0.000005 ($n = 35$; 1 s.d.), which matches the certified value of 0.71034 ± 0.00026. Internal precision (1 s.d.) on the isotope ratio measurements was in all cases better than 0.000043, and averaged 0.000005. Replicate lab-processed samples indicated that external precision was similar to the analytical precision (±0.000006, $n = 6$).

2.2. Study areas

Samples were collected from a variety of sites worldwide (Fig. 1), which were chosen to encompass a diversity of relevant aquifer lithologies (Table 1). These include carbonate bedrock and clastic sediments, basaltic lava flows, igneous intrusive rocks such as granites, island arc suites of quartz diorites, granodiorites, and basaltic andesites, as well as mixed lithology glacial till. SGD has been studied extensively at most of these sites, ensuring that samples collected for this study are representative of global SGD inputs. In general, samples were collected from surface waters and surficial (shallow, <10 m depth) aquifers, though some samples (e.g., an artesian well in Venice) were obtained from deeper wells. Some sites were targeted because they have previously been identified as major sources of Sr that is isotopically distinct from seawater Sr (the Yucatan Peninsula and the Ganges–Brahmaputra drainage basin; Basu et al., 2001; Perry et al., 2009).The Ganges–Brahmaputra drainage basin is primarily made up of igneous and metamorphic rocks, including granites and gneiss, although some sandstones, carbonates, shales, and conglomerates are present (Alam et al., 2003). The igneous and sedimentary bedrock of this basin is characterized by the occurrence of highly radiogenic source rocks and minerals, imparting high $^{87}Sr/^{86}Sr$ values (~0.77) to water draining the region (e.g., Edmond, 1992; Krishnaswami et al., 1992; Blum et al., 1998; Galy et al., 1999). The floodplain alluvial soils in the delta comprise a mixture of silts, clays, quartz, and carbonates (Coleman, 1969; Brammer et al., 1988; Uddin and Lundberg, 1998). The northeast USA (Great South Bay, NY; Pamet River, MA; Waquoit Bay, MA) sites are characterized by glacial till deposits with subterranean estuaries comprising unconsolidated sands of quartz and other minerals (e.g., Cambareri and Eichner, 1998). Reported $^{87}Sr/^{86}Sr$ ratios in groundwater at the NY and MA sites are ~0.71, close to the global seawater value (Xin, 1993; Bau et al., 2004). The complex geology of western Panama is poorly studied. The aquifer solids are eroded from quartz diorites, granodiorites, and basaltic andesites from a submarine island arc system (Coates et al., 2004). Mauritius Island is composed of young basaltic lava flows (<0.7 Ma for the Younger series that comprises the main aquifer) with less radiogenic $^{87}Sr/^{86}Sr$ ratios (~0.704; Nohda et al., 2005). The Pliocene (5 Ma) carbonate rocks that make up the Yucatan Peninsula, Mexico, have $^{87}Sr/^{86}Sr$ ratios less radiogenic (0.708) than present day seawater (Perry et al., 2009). Due to extensive dissolution of the carbonate bedrock and evaporite deposits by infiltrating rainwater, groundwater Sr concentrations are elevated and display $^{87}Sr/^{86}Sr$ ratios similar to the carbonates and evaporites (Perry et al., 2009). The groundwater samples from Florida were collected in the shallow aquifer from unconsolidated Holocene sediments. The deeper Floridan aquifer comprises Tertiary limestone and dolomite (Hickey et al., 2010). The Venice Lagoon is underlain by sand and clay layers of alluvial and marine origin, with Pliocene carbonate bedrock beneath (Brambati et al., 2003).

3. RESULTS

Measured Sr data and sample salinities are compiled in Table 2.

3.1. Sr concentrations

Strontium concentrations generally showed conservative mixing patterns relative to salinity at our study sites (Fig. 2). There was substantial variability in both the seawater (60–90 μM; salinity ~30) and meteoric groundwater or river end-members among the sites (0.1–24.4 μM;

Table 2
Dissolved Sr concentrations, Sr isotope ratios, and salinity in groundwater and surface water.

Sample site & Type	Sample ID	$^{87/86}$Sr	±	Salinity	Sr (μM)*	1/Sr (μM^{-1})
Bangladesh						
Bay of Bengal	BBG 72-0	0.709185	0.000002	29.6	75	0.0134
	BG 66-0	0.709181	0.000006	30.0	77	0.0130
	BG 72-35	0.709170	0.000003	30.2	85	0.0118
	BG 64-35	0.709170	0.000005	30.7	84	0.0119
	BG 9-20	0.709176	0.000004	31.0	77	0.0130
Sandwip Channel	BG 124	0.709407	0.000004	12.7	32	0.0313
	BG 120	0.709364	0.000003	14.4	36	0.0276
	BG 3-0	0.709262	0.000004	19.3	48	0.0207
	BG 9-0	0.709194	0.000003	28.6	72	0.0139
	BG 15-0	0.709177	0.000003	29.8	78	0.0129
	BG 5-0	0.709180	0.000003	31.5	79	0.0126
Shabazpur (River)	BG 18-0	0.709232	0.000006	24.5	59	0.0169
	BG 21-0	0.709259	0.000003	20.4	54	0.0186
	BG 23-0	0.709301	0.000006	15.7	48	0.0210
	BG 26-0	0.709530	0.000004	10.7	28	0.0363
	BG 28-0	0.709946	0.000005	5.9	16	0.0620
	BG 31-0	0.710896	0.000005	2.9	7.9	0.1263
	BG 148	0.722111	0.000009	0.0	0.94	1.0665
Florida						
	RB2	0.709124	0.000006	9.45	32	0.0312
	RB3	0.709031	0.000005	7.94	29	0.0349
	RB4	0.709106	0.000004	4.89	15	0.0681
	RB5	0.709082	0.000005	2.81	8.7	0.1148
	RT12	0.709176	0.000005	35.9	85	0.0118
	RBA	0.709134	0.000003	11.9	32	0.0315
	RBB	0.709144	0.000003	21.3	53	0.0187
	RBF	0.709152	0.000004	28.9	68	0.0147
Panama						
	LJL 113	0.709143	0.000005	0.72	8.2	0.1223
	LJL 123	0.709134	0.000004	10.0	8.5	0.1176
	LJL 114	0.709153	0.000006	14.8	17	0.0589
	LJL 115	0.709147	0.000003	21.1	39	0.0259
	LJL126	0.709067	0.000004	16.6	24	0.0410
	LJL127	0.707587	0.000043	0.33	0.22	4.6006
	LJL128	0.708623	0.000038	1.23	0.66	1.5146
	LJL124	0.709158	0.000005	26.2	29	0.0348
	LJL135	0.709173	0.000004	30.5	56	0.0178
	LJL121	0.709186	0.000006	28.9	39	0.0255
Pamet River, MA						
	PR586	0.709183	0.000009	0.28	0.12	8.5755
	PR588	0.709245	0.000004	3.88	12	0.0833
	PR591	0.709215	0.000005	9.41	30	0.0328
	PR595	0.709213	0.000003	12.6	37	0.0269
	PR601	0.709168	0.000002	24.5	65	0.0155
	PR568	0.709184	0.000005	17.8	40	0.0253
	PR569	0.709187	0.000004	24.5	61	0.0165
	PR575	0.709185	0.000005	30.3	69	0.0144
	PR756	0.709167	0.000004	30.4	69	0.0144
Mauritius						
	MR4	0.708985	0.000003	2.55	13	0.0756
	MR7	0.708827	0.000002	7.28	22	0.0451
	MR7	0.708829	0.000004	7.28	22	0.0451
	MR12	0.709030	0.000003	16.7	46	0.0217
	MR14	0.709122	0.000006	22.8	57	0.0175
	MRU16	0.708665	0.000004	0.0	8.1	0.1236
	MRU5	0.708957	0.000004	3.76	15	0.0679
	MRU6	0.708933	0.000003	14.2	29	0.0345
	MRU8	0.708828	0.000006	3.04	11	0.0920

(*continued on next page*)

Table 2 *(continued)*

Sample site & Type	Sample ID	$^{87/86}Sr$	±	Salinity	Sr (μM)*	1/Sr (μM^{-1})
	MRU2	0.709166	0.000002	27.0	60	0.0165
	MRU1	0.709168	0.000004	31.8	74	0.0136
Waquoit Bay, MA						
Bay surface	WBS-1	0.709106	0.000004	20.5	45	0.0220
	WBS-6	0.709152	0.000004	29.6	66	0.0153
	WBS-15	0.709170	0.000004	30.3	67	0.0148
Subterranean estuary	WB6-33	0.709260	0.000008	0.23	0.33	2.9882
	WB6 44	0.709184	0.000004	4.2	8.6	0.1161
	WB6 45	0.709176	0.000003	7.67	18	0.0543
	WB6 52	0.709172	0.000003	25.8	65	0.0154
	WB6-46	0.709186	0.000002	16.8	35	0.0283
Yucatan						
Sabtun Cenote	YT 2-4	0.708010	0.000006	2.0	31	0.0318
	YT 11	0.708228	0.000005	5.0	54	0.0186
	YT 12	0.708400	0.000005	10	68	0.0148
	YT 10	0.708533	0.000005	15	93	0.0107
	YT 14	0.708610	0.000005	20	124	0.0080
	YT 13	0.708664	0.000005	25	152	0.0066
	YT 15	0.708717	0.000003	36	194	0.0052
Celestún Lagoon	YT57	0.708834	0.000004	20.6	80	0.0124
	YT58	0.708484	0.000002	17.8	107	0.0093
	YT54	0.709152	0.000002	33.7	86	0.0116
Other cenotes and groundwater	YT3	0.708288	0.000004	6.9	57	0.0176
	YT5	0.708276	0.000005	17.0	99	0.0101
	YT6	0.708406	0.000004	7.2	46	0.0218
	YT30	0.709262	0.000004	27.7	68	0.0148
Venice Lagoon						
Silone Channel	A2	0.708290	0.000004	0.8	3.9	0.2586
	A4	0.708790	0.000005	2.8	9.4	0.1069
	A5	0.708852	0.000002	4.1	13	0.0781
	A6	0.708985	0.000004	7.7	19	0.0517
	A1	0.709109	0.000004	16.5	38	0.0262
	B1	0.709098	0.000005	21.8	31	0.0319
Surface	B5	0.709144	0.000006	24.5	51	0.0194
	B3	0.709147	0.000002	27.6	59	0.0169
	B4	0.709155	0.000004	29.2	59	0.0168
	4 miles	0.709163	0.000003	34.4	69	0.0146
Groundwater at Punta Sabbione	VP-01	0.709156	0.000001	12.9	31	0.0321
	VP-03	0.709155	0.000003	14.4	34	0.0290
	VP-05	0.709149	0.000004	16.6	38	0.0266
	VP-06	0.709149	0.000006	18.9	44	0.0225
	VP-08	0.709153	0.000005	21.3	48	0.0208
	VP-17	0.709162	0.000006	23.5	55	0.0182
	VP-19	0.709162	0.000003	23.5	55	0.0181
	VP-22	0.709162	0.000005	24.4	61	0.0164
	VP-15	0.709157	0.000002	27.1	68	0.0147
	VP-10	0.709169	0.000004	28.5	62	0.0160
Treporti	Trep-1	0.709158	0.000004	41.8	95	0.0105
	Trep-2	0.709165	0.000007	42.4	95	0.0105
Artesian	ILC-1	0.708218	0.000009	0.7	4.5	0.2246
Great South Bay, NY						
Carmans River	GSB-01	0.709586	0.000007	4.37	12	0.0817
	GSB-01	0.709284	0.000003	4.37	12	0.0817
	GSB-02	0.709208	0.000005	12.7	37	0.0271
	GSB-04	0.709173	0.000004	22.2	59	0.0171

(*continued on next page*)

Table 2 (*continued*)

Sample site & Type	Sample ID	$^{87/86}Sr$	±	Salinity	Sr (μM)*	1/Sr (μM^{-1})
Connetquot River	GSB-11	0.710095	0.000003	0.86	3.2	0.3107
	GSB-11	0.710092	0.000004	0.86	3.2	0.3107
	GSB-12	0.709433	0.000004	3.12	10	0.0968
	GSB-13	0.709311	0.000005	5.07	16	0.0621
	GSB-14	0.709243	0.000001	8.74	27	0.0372
	GSB-16	0.709195	0.000004	16.3	49	0.0206
	GSB-18	0.709180	0.000004	20.2	61	0.0163
Bay surface	GSB-10	0.709189	0.000004	24.6	70	0.0144
	GSB-36	0.709169	0.000004	26.7	80	0.0126
	GSB-19	0.709172	0.000004	29.5	78	0.0128
	GSB-27	0.709163	0.000005	31	86	0.0116
Subterranean Estuary at	B-01	0.709173	0.000005	29.0	82	0.0123
Roe Avenue	B-03	0.709170	0.000004	26.1	74	0.0135
	B-04	0.709164	0.000004	21.4	57	0.0175
	B-05	0.709170	0.000004	17.5	50	0.0201
	B-06	0.709163	0.000004	11.7	34	0.0290
	B-07	0.709182	0.000004	6.32	19	0.0528
	B-08	0.709352	0.000006	0.5	1.9	0.5242
	B-13	0.709397	0.000008	0.3	1.4	0.7246
Fresh seep	Seep	0.709185	0.000005	0.1	2.4	0.4222

* Sr concentration measurements have a standard deviation of less than 3%.

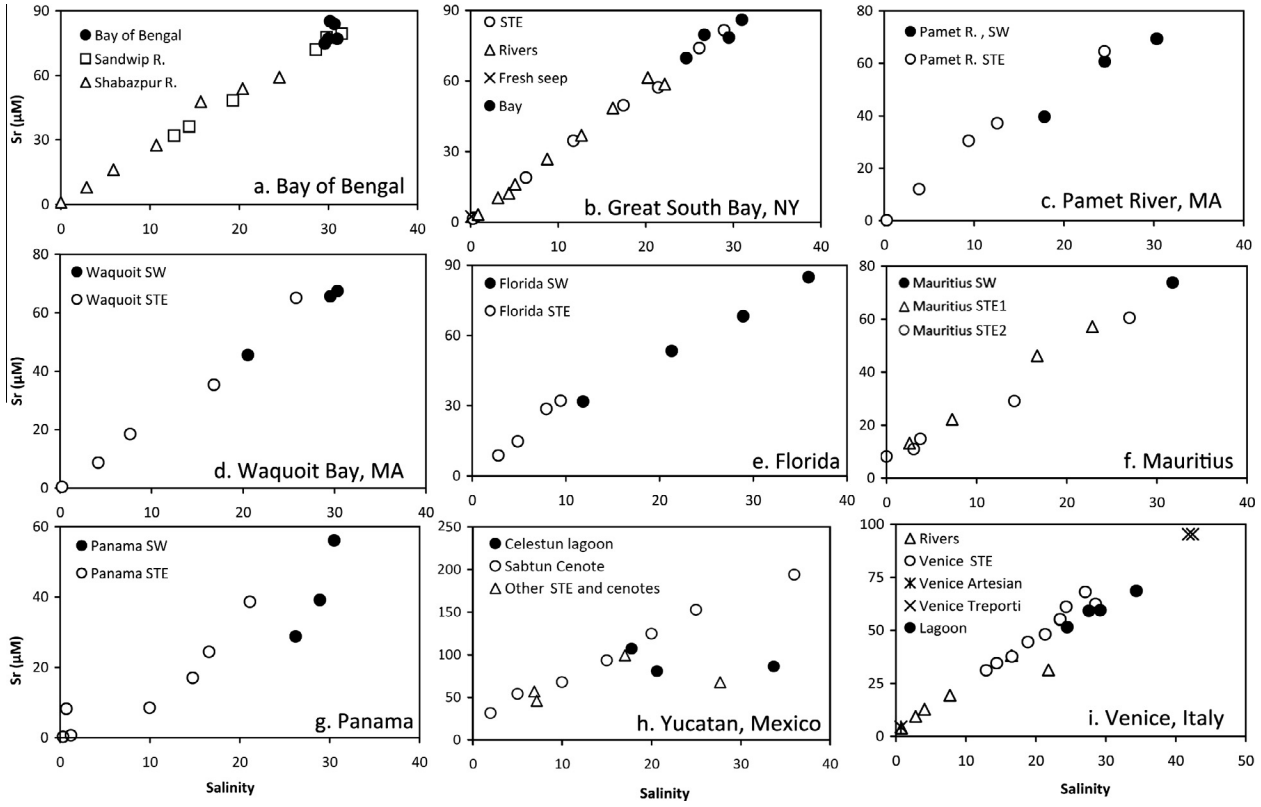

Fig. 2. Co-variation of total dissolved Sr with salinity. Individual figure legends explain the symbols, and site locations are labeled on the graphs. Note that *y*-axis scales vary among the graphs.

salinity < 1), reflecting different local sources, but Sr mixing behavior within sites was consistently linear.

Two sites stand out: Yucatan and Panama. Samples from the Yucatan Sabtún cenote were highly enriched in Sr (24.4–194 μM; salinity 0–36; Fig. 2h) relative to other locations, although Sr mixing behavior in the cenote was similarly conservative. The seawater end-member concentration was consistent with other locations (86 μM; salinity 33.7), but mid-salinity concentrations in lagoon surface water showed pronounced enrichment that matched the

levels observed in the Sabtún cenote and other groundwaters. At the Panama site, seawater Sr concentrations were somewhat lower than other locations (56 μM; salinity 30.5), and Sr in both STE samples and surface water showed non-linear mixing behavior (Fig. 2g). Although Sr patterns for both types of Panama samples were concave upward, maximum removal occurred at different salinities.

3.2. Sr isotope ratios

$^{87}Sr/^{86}Sr$ ratios in groundwaters from different geologic settings varied greatly (Fig. 3). In most cases, the meteoric groundwater or surface water end-member was very different from the seawater end-member ratio. Seawater end-members were generally similar to the global ocean $^{87}Sr/^{86}Sr$ average of ~0.70916 (Fig. 3; Table 2; Hess et al., 1986; Veizer, 1989; Hodell et al., 1991; Paytan et al., 1993; Henderson et al., 1994; Farrell et al., 1995). Strontium isotope mixing behavior was conservative (within the analytical precision) in surface waters from, for example, the Bay of Bengal (Fig. 3a), Great South Bay (Fig. 3b), and the Venice Lagoon (Fig. 3i). At most sites, however, $^{87}Sr/^{86}Sr$ distributions in the STE showed marked but variable degrees of non-conservative behavior (Pamet River, Waquoit Bay, Florida, Mauritius, and Yucatan). This non-conservative behavior uniformly favored the meteoric groundwater end-member. For example, at the Florida site (Fig. 3e), the meteoric groundwater end-member was less radiogenic than seawater, and $^{87}Sr/^{86}Sr$ ratios in the STE exhibited a concave-downward pattern. Panama (Fig. 3g) was the only site with two-endmember mixing in the STE that exhibited conservative behavior of $^{87}Sr/^{86}Sr$ ratios. In the STE at Venice and Great South Bay (GSB) sites, $^{87}Sr/^{86}Sr$ mixing patterns between surface water and groundwater indicated multiple meteoric end-members with unique $^{87}Sr/^{86}Sr$ values. In both cases, one meteoric end-member was substantially different from seawater (e.g., in GSB, 0.7100; Fig. 3b), while the other was more similar to seawater (in GSB, 0.7093). Shallow groundwater at both sites had a $^{87}Sr/^{86}Sr$ signature similar to seawater, while river waters had signatures very different from seawater. At the Yucatan site, Sabtún cenote samples showed coherent, slightly non-conservative mixing behavior of $^{87}Sr/^{86}Sr$ ratios, while data for other samples were scattered (Fig. 3h).

4. DISCUSSION

4.1. Sr in the subterranean estuary

Evidence from Sr concentrations at these sites indicated that Sr mixes conservatively in the subterranean estuary. Reanalysis of the Waquoit Bay samples reported by Charette and Sholkovitz (2006) revealed a conservative mixing pattern; the earlier study that reported non-conservative mixing did not analyze Sr via high-precision isotope dilution, which may explain the discrepancy with the data reported in this

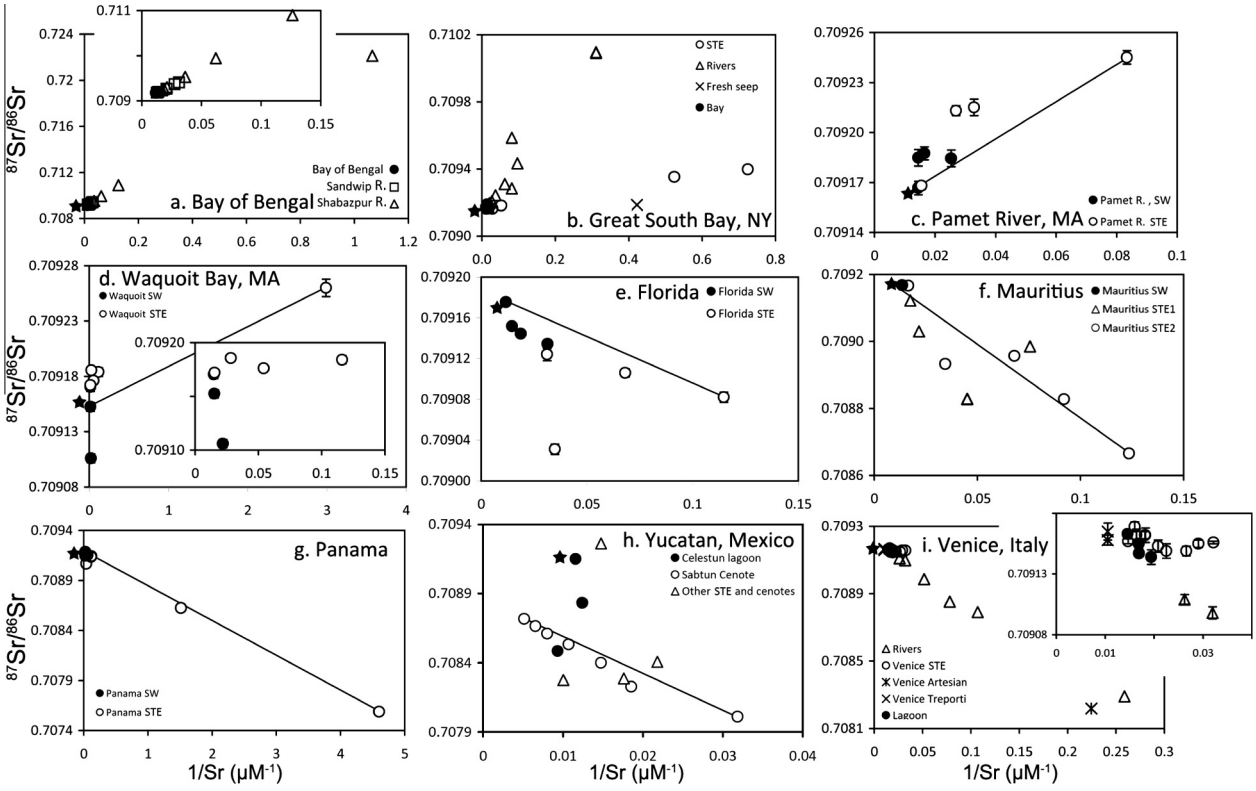

Fig. 3. $^{87}Sr/^{86}Sr$ systematics. Symbols as in Fig. 2; star-shaped symbols indicate the approximate composition of global average seawater ($^{87}Sr/^{86}Sr = 0.70916$, $1/Sr = 0.01\ \mu M^{-1}$). Insets show expanded views near the origin. Diagonal lines indicate conservative mixing between meteoric groundwater and seawater end-members at the six STE sites where 3-endmember mixing was not indicated (i.e., excluding GSB and Venice). Isotope ratio uncertainties are drawn on these plots, but where error bars are not visible, they are smaller than the symbol size.

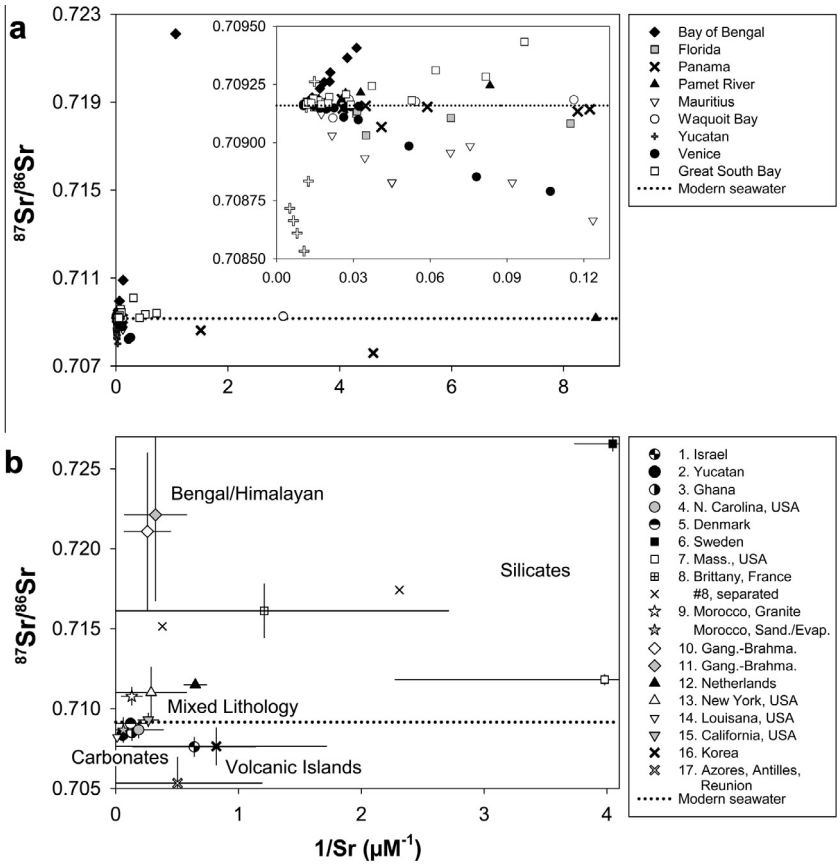

Fig. 4. (a) Compiled $^{87}Sr/^{86}Sr$ data from the present study. The dashed line indicates the $^{87}Sr/^{86}Sr$ ratio of global average seawater. (b) Sr isotope ratios in diverse, near-coastal meteoric groundwaters. Common aquifer lithologies are indicated (References: 1. Starinsky et al. (1980); 2. Perry et al. (2009); 3. Jørgensen and Banoeng-Yakubo (2001); 4. Woods et al. (2000); 5. Jørgensen et al. (2008); 6. Land et al. (2000); 7. Bau et al. (2004); 8. Widory et al. (2004); 9. Bouchaou et al. (2008); 10. Dowling et al. (2003); 11. Basu et al. (2001); 12. Petelet-Giraud et al. (2009); 13. Siegel et al. (2000); 14. Huff and Bonck (1993); 15. Vengosh et al. (2002); 16. Kim et al. (2003); 17. Louvat and Allègre (1998) and Rad et al. (2007).

study. Strontium concentration trends at the Panama site did show removal of Sr in the STE (Fig. 2g), with an end-member concentration of ~32 μM (i.e., removal of 32 μmol Sr L^{-1} from seawater during recirculation, based on the apparent zero-salinity end-member). The process controlling this removal is not obvious from the current dataset, although scavenging onto authigenic iron oxides may play a role (Andersson et al., 1994). Sorption by Fe-oxyhydroxides may be especially important in the STE, due to extensive formation of such precipitates during mixing of meteoric and marine groundwaters (Charette and Sholkovitz, 2002; Charette et al., 2005; Spiteri et al., 2006). However, Sr removal from solution by this mechanism does not appear to be ubiquitous, given that Sr depletion was not evident at some sites where Fe precipitation has been clearly documented (e.g., Waquoit Bay and Great South Bay; Charette and Sholkovitz, 2006; Beck et al., 2010).

The vast Sr enrichment in groundwater observed at the Yucatan site has been reported previously (Perry et al., 2002; Young et al., 2008), and is the result of evaporite (gypsum, celestite) and carbonate dissolution in the aquifer (Perry et al., 2009). The good match between Sr enrichment in surface waters of the Celestún Lagoon and the cenote trends (Fig. 2h) indicates that the enrichment may be caused by mixing with water from the Sabtun cenote, and that the cenote source may satisfy the "brackish groundwater" end-member hypothesized by Young et al. (2008). This is the only site in the current dataset where groundwater discharge is obvious in surface water Sr concentrations. This is not surprising given the high groundwater Sr concentrations at this site, but it does highlight that Sr-rich groundwater from certain types of coastal aquifers (e.g., carbonate) may contribute a greater proportion of the global SGD-driven Sr flux than other geologic settings.

The compiled data show that the Sr concentrations in coastal meteoric groundwater and surface water (i.e., river) end-members are not greatly different from each other (e.g., Fig. 2b and i). Thus, except for locations where Sr-enriched hydrothermal fluids have interacted with unradiogenic basaltic bedrock (Allègre et al., 2010), or where dissolution of carbonates and evaporites enriches the groundwater in Sr (Perry et al., 2009), SGD does not contain unusually high concentrations of dissolved Sr. As such, SGD is not likely to greatly elevate coastal strontium concentrations in most regions. Nonetheless, because karstic coastlines (25% of global coastal geomorphology; Ford and Williams,

2007) and volcanic islands host exceptionally large volumes of SGD (1/3 of the global flux, Zektser et al., 2006; Allègre et al., 2010), such inputs warrant more scrutiny as significant components of the Sr budget in the global ocean (Allègre et al., 2010).

4.2. $^{87}Sr/^{86}Sr$ trends

The $^{87}Sr/^{86}Sr$ results showed that ratios typically mixed non-conservatively in the STE (Fig. 3; with the Panama site the sole exception, Fig. 3g). In all cases, the trends indicated non-conservative input of Sr with a ratio similar to that of the meteoric groundwater end-member. However, the conservative mixing behavior of Sr concentrations suggests that the non-conservative $^{87}Sr/^{86}Sr$ ratio patterns are the result of Sr exchange between seawater Sr in solution and groundwater Sr adsorbed on aquifer solids. Thus, brackish groundwater that discharges carries Sr that is isotopically more similar to that found in local meteoric groundwater. Recent data from western India indicate that isotope exchange end-members in SGD may vary temporally (Rahaman and Singh, 2012), although it is not clear how common this phenomenon is or how it might be incorporated into a global flux model. While different from the non-conservative Sr input hypothesized by Cochran et al. (2003), isotope exchange would have the same net effect of augmenting the brackish groundwater end-member. Strontium isotope exchange in the STE potentially represents a major component of the marine Sr isotope budget because brackish SGD represents a much larger flux than meteoric SGD (approximately 10-fold higher; Burnett et al., 2003, 2006).

Two of the study sites had $^{87}Sr/^{86}Sr$ trends that clearly indicated mixing of more than two end-members. GSB (Fig. 3b) and Venice (Fig. 3i) had three of the same end-members: (1) seawater, (2) meteoric groundwater with seawater-like $^{87}Sr/^{86}Sr$ ratios, and (3) groundwater or river water with distinct $^{87}Sr/^{86}Sr$ signature. At the Venice site, this latter end-member was less radiogenic (0.7082) than seawater, compared with the more-radiogenic signature of GSB (0.7101). These differences are easily explained by different aquifer lithologies. In these three cases, the shallow coastal groundwater had lower Sr concentrations than local rivers, and very different $^{87}Sr/^{86}Sr$ ratios. In Venice, shallow meteoric groundwater was not sampled, but its influence on the $^{87}Sr/^{86}Sr$ ratio is indicated by brackish groundwater samples (Fig. 3i, inset). In GSB (Fig. 3b), a free-flowing spring above the high tide line also had a composition (2.4 μM, 0.7092) more similar to the shallow low-salinity porewater (1.4 μM, 0.7094) than rivers (3.2 μM, 0.7101). The $^{87}Sr/^{86}Sr$ signature of the spring implies that the dominant source of Sr to shallow groundwater is probably sea salt aerosol collected by rainwater that recharges the surficial, unconfined aquifer (Xin, 1993; Siegel et al., 2000). At the Venice site, the Sr signature (4.5 μM, 0.7082) of deep groundwater from an artesian well (located on Isola La Cura, screened at 300 m depth, flow rate 50,000 L d^{-1}; Rapaglia, 2005) matched very well that of local rivers (3.9 μM, 0.7083), indicating that both are the result of leaching from aquifer carbonates, not aerosol inputs. The $^{87}Sr/^{86}Sr$ of hypersaline groundwater at the Venice-Treporti site was indistinguishable from seawater, in agreement with a previous report that seawater flows lagoon-ward along permeable paleo-inlets under the barrier island at this location (Rapaglia et al., 2010).

4.3. Controls on groundwater Sr

Shallow (1–2 m) coastal groundwater can apparently be affected by aerosol-derived Sr accumulated during recent recharge. However, for deeper meteoric groundwaters, leaching and dissolution of aquifer rocks gives groundwater its characteristic isotopic composition and concentration (McNutt, 2000). From the data compiled in Fig. 4a, it is obvious that the sites chosen here reflect a variety of local lithologies with Sr inputs that are either more or less radiogenic than seawater Sr, and which trend approximately linearly toward a common seawater signature during mixing in the subterranean estuary. These patterns match exactly those reported in other Sr isotope groundwater studies at near-coastal, inland sites (Fig. 4b).

Aquifers dominated by old silicate rocks such as granites and gneisses host groundwaters that are much more radiogenic than seawater (up to 0.73), but have low Sr concentrations (<1 μM). Carbonate-dominated and volcanic island aquifers contain groundwater with relatively high concentrations of Sr that is less radiogenic than seawater. Primary marine carbonates have $^{87}Sr/^{86}Sr$ values lower than present-day seawater that reflect the less-radiogenic $^{87}Sr/^{86}Sr$ composition of paleo-seawater in which they formed, and young volcanic basalts have less radiogenic Sr owing to the recent extraction of lavas from the Earth's mantle. Groundwater from volcanic island aquifers tends to have a lower Sr concentration than groundwater from carbonate aquifers (<5 vs. >5 μM, respectively). Although thermal springs on volcanic islands may have much higher Sr concentrations than ambient temperature groundwater, (up to 140 vs. ~5 μM, respectively, in the Azores and Antilles; Louvat and Allègre, 1998; Rad et al., 2007), this is not necessarily always the case (Sr < 1 μM, Iceland; Elderfield and Greaves, 1981).

Groundwaters from the Bengal Basin have very high Sr concentrations (2–10 μM), and also exceptionally high $^{87}Sr/^{86}Sr$ ratios (up to 0.735; Basu et al., 2001; Dowling et al., 2003). There is some controversy regarding the source of highly radiogenic Sr, but it seems to be a product of both carbonate and silicate weathering, with the latter supplying the most radiogenic Sr (Edmond, 1992; Krishnaswami et al., 1992; Blum et al., 1998; Dowling et al., 2003; Tripathy and Singh, 2010). Interestingly, coastal groundwaters in the Bengal Basin seem to be more influenced by carbonate weathering, and consequently have lower $^{87}Sr/^{86}Sr$ ratios than elsewhere in the region (<0.717; Dowling et al., 2003).

Our data from the Bangladesh site (Figs. 2a and 3a) indicate conservative behavior of Sr concentrations and $^{87}Sr/^{86}Sr$ ratios during mixing between river and coastal waters, and show no evidence for excess Sr input from SGD. Mid-salinity samples from the Sandwip Channel (Bangladesh) correspond to the highly Ba- and Ra-enriched samples of Carroll et al. (1993). Although the latter tracers

Table 3
Parameters for the marine $^{87}Sr/^{86}Sr$ budget.

Source	Dissolved Sr concentration (μM)	$^{87}Sr/^{86}Sr$	Sr flux (10^{10} mol y^{-1})	Inventory (10^{15} mol)	Proportion of marine isotope budget (%)*	Ref.
Rivers	0.902	0.7116	3.40		–	[a]
	0.89	0.7119	3.33		–	[b]
	0.5	0.7131	1.88		–	[c]
	1.22	0.7111	4.70		100	[d] **
Sedimentary diagenesis		0.7084	0.34		−3	[e]
Hydrothermal input		0.7025	0.31		−23	[f]
Seawater	87.4[f]	0.70916	–	116[g]		
Meteoric SGD	2.9	0.7089	0.71		between −2 and −8	This work
Brackish SGD (with isotope exchange; $S = 10$)	28 ± 5	0.7091	16–35‡		between −11 and −23	This work

* Positive and negative values indicate more radiogenic or less radiogenic source terms, respectively, relative to seawater.
** River source term parameters used in $^{87}Sr/^{86}Sr$ budget to calculate SGD input.
‡ Note that the brackish SGD flux represents recirculated seawater, and while it is isotopically distinct from seawater, it does not represent a net flux of Sr to the ocean.
[a] Davis et al. (2003).
[b] Palmer and Edmond (1989).
[c] Allègre et al. (2010).
[d] Peucker-Ehrenbrink et al. (2010).
[e] Elderfield and Gieskes (1982), as reported by Davis et al. (2003).
[f] de Villiers (1999).
[g] Calculated with data from de Villiers (1999) and Charette and Smith (2010).

indicated elevated SGD in this region (Moore, 1997), the input does not appear to have affected Sr. This is consistent with the fact that seawater recirculation comprises the major fraction of SGD (e.g., Li et al., 1999), and that both Ba and Ra are highly enriched in brackish groundwater (Charette and Sholkovitz, 2006; Moore and Shaw, 2008), while Sr is apparently not. It is clear from this example that estimation of SGD-driven Sr flux is not necessarily straightforward, and this may be especially true for the Bay of Bengal. Indeed, even making SGD volume flux estimates at this location is apparently difficult (Harvey, 2002). Because the Sr concentrations and $^{87}Sr/^{86}Sr$ ratios at this site appear to be uniquely high, constraining the Sr flux via SGD in this region will probably be critical for an accurate global Sr budget.

In mixed lithology aquifers, such as the glacial-till dominated northeast US and alluvial aquifers in other locations, the Sr composition of the groundwater may reflect a combination of weathering several types of substrate. Even very small amounts of carbonate in mixed lithology aquifers can control the Sr content and $^{87}Sr/^{86}Sr$ composition of the groundwater because carbonate dissolution supplies such large quantities of Sr to solution (McNutt, 2000). In the Massachusetts and New York (US) sites examined here, carbonate dissolution does not appear to play a large role in contributing Sr to the groundwater, and $^{87}Sr/^{86}Sr$ ratios reflect input from silicate weathering (Fig. 4a). In other locations where aquifers contain carbonates, Sr concentrations and $^{87}Sr/^{86}Sr$ ratios are more similar to marine carbonates and seawater (Fig. 4b).

It is possible for anthropogenic contamination to influence the Sr composition of coastal groundwater, as has been shown in surface waters (Négrel and Deschamps, 1996; Négrel, 1999; Böhlke and Horan, 2000). Data from a granitic gneiss aquifer in Brittany, France (Widory et al., 2004) are plotted in Fig. 4b. The data have also been separated (asterisks without error bars in Fig. 4b) into uncontaminated samples, which have lower Sr concentrations and higher $^{87}Sr/^{86}Sr$ ratios, and samples contaminated by agricultural activities (fertilizer, manure, and sewage), which have higher Sr content and lower $^{87}Sr/^{86}Sr$ ratios. We find no evidence of such contamination in our dataset, but much of the SGD literature has demonstrated input of nutrient-contaminated groundwater to the coastal ocean. However unlikely, input of "anthropogenic Sr" may be a non-negligible, and potentially increasing, component of the modern coastal ocean $^{87}Sr/^{86}Sr$ budget.

The Yucatan is the only site in the current dataset where SGD input of Sr is evident from elevated concentrations in surface waters (Fig. 2h), and indeed, is the site where we would expect the SGD source to be most visible. The unique characteristics of this site result in mixing of three end-members: meteoric groundwater with low $^{87}Sr/^{86}Sr$ and high Sr concentrations, saline groundwater with very high Sr concentrations and low $^{87}Sr/^{86}Sr$, and average seawater. This three-endmember mixing can generally explain the scatter in the Sr ratio data at the Yucatan site (Fig. 3h), although variability in $^{87}Sr/^{86}Sr$ patterns of different groundwaters is a complication. Small groundwater inputs to the lagoon can be observed in the presence of the large seawater background because meteoric and brackish groundwaters are highly enriched in Sr at this site (~24 μM at zero salinity). In contrast, at most locations,

Table 4
Sr composition of groundwater in different lithology aquifers, and contribution of different lithology sources to the global SGD Sr source.

	End-member values[a]		%Vol. flux	%SGD Sr flux	%Ratio flux[b]
	$^{87}Sr/^{86}Sr$	Sr (μM)			
Carbonate	0.708	10	12	40	−54
Shale	0.711	2	15	10	29
Sandstone	0.710	3	11	12	15
Extrusive igneous	0.706	2	17	11	−42
Shield (granite)	0.713	0.5	11	2	11
"Complex"	0.709	2	32	22	−4
Ganges–Brahamaputra	0.720	6	1	3	45

[a] End-members are estimated from literature reports of groundwater Sr and $^{87}Sr/^{86}Sr$ measurements. Only non-saline, uncontaminated groundwaters were considered. See Fig. 4 for references; additional references include McNutt et al. (1987), Vengosh et al. (1999), Hogan et al. (2000), Vilomet et al. (2001), Frost et al. (2002), Wiegand et al. (2002), Gosselin et al. (2004), Frost and Toner (2004), Vengosh et al. (2005), Jacobson and Wasserburg (2005), Helstrup (2006), Vengosh et al. (2007), Klaus et al. (2007), Cartwright et al. (2007), Sultan et al. (2008), Möller et al. (2008), Shand et al. (2009), Raiber et al. (2009) and Gilli et al. (2009).

[b] Negative numbers indicate Sr sources with isotope ratios that are less radiogenic than seawater, whereas positive numbers indicate sources that are more radiogenic than seawater. This column illustrates how much aquifers of each lithology contribute to the model-estimated global flux.

Sr concentrations in groundwater are similar to those in surface freshwater, and Sr-salinity trends in surface water are linear.

4.4. The Sr isotope mass balance in the ocean

The results of this study can be used to refine estimates of SGD as a component of the oceanic $^{87}Sr/^{86}Sr$ budget. The mass balance for Sr in the ocean is given by:

$$I_{SW}\left(\frac{dR_{SW}}{dt}\right) = \sum_i J_i(R_i - R_{SW}) \quad (1)$$

where the left side of the equation is the product of Sr inventory in the ocean and the rate of change of the $^{87}Sr/^{86}Sr$ ratio, and the right side of the equation is the sum of Sr input fluxes to the ocean (mass fluxes multiplied by the difference of their isotope ratios and that of modern seawater), with subscript i representing sources from rivers, diffusive diagenetic fluxes from sediments, hydrothermal processes, and SGD, and subscript SW denoting seawater. At steady state (i.e., $dR/dt = 0$), Sr sources that are more radiogenic than seawater balance less-radiogenic sources. Strontium isotope sources and characteristic signatures are shown in Table 3. Excluding for the moment SGD, the Sr budget is clearly dominated by radiogenic Sr input from rivers. Thus, uncertainty in the river Sr flux and end-member $^{87}Sr/^{86}Sr$ ratio will contribute significantly to uncertainty in any SGD estimate. Although river systems may be the most accessible and easily sampled, there is much reason for imprecision of Sr flux estimates, including seasonality of river flow, anthropogenic contamination, insufficient sampling of drainage basins, and temporal variability in river Sr composition (discussed in detail by Peucker-Ehrenbrink et al., 2010). Table 3 shows two similar and often-cited estimates of river input (Palmer and Edmond, 1989; Davis et al., 2003). These contrast with two more recent values that are very different from both the earlier estimates and each other (Allègre et al., 2010; Peucker-Ehrenbrink et al., 2010). Allègre et al. (2010) used recent data for large rivers to update previous estimates, and arrived at a lower Sr flux (1.88×10^{10} vs. 3.4×10^{10} mol y^{-1}) with a substantially more-radiogenic signature (0.7136 vs. ~0.7116) for large continental rivers. If contributions from thermal springs and underground water to rivers draining island arcs are included, the Allègre et al. (2010) river estimate yields 1.98×10^{10} mol Sr y^{-1} with an $^{87}Sr/^{86}Sr$ value of 0.71308, a value significantly more radiogenic than most previous estimates of river runoff. In contrast, Peucker-Ehrenbrink et al. (2010) developed a riverine Sr flux model based on consideration of drainage basin geology. Their model accounts for undersampled or previously neglected rivers, and they estimated a high Sr mass flux (4.7×10^{10} mol y^{-1}) with a relatively non-radiogenic isotopic composition (0.7111). These differing literature values lead to substantial variability in calculation of the possible SGD end-member. Thus, choice of the river source is important, though somewhat subjective. Nonetheless, we feel Peucker-Ehrenbrink et al. (2010) provide the best estimate, as it is the most recent, complete, and thorough treatment of fluvial Sr inputs.

Diffusive diagenesis and hydrothermal fluxes are taken from Elderfield and Gieskes (1982) and Davis et al. (2003), respectively. The submarine hydrothermal flux includes high- and low-temperature axial and arc-related inputs.

4.4.1. SGD-driven Sr flux – Meteoric groundwater discharge

Global SGD-driven Sr input was estimated using a simple model that combines meteoric groundwater flux with estimates of Sr concentration and $^{87}Sr/^{86}Sr$ composition in groundwater from different aquifer types. Before describing the model, it is important to note that this assessment provides only a very coarse approximation of the SGD-driven Sr flux. The estimate is based on the best currently-available data; however, there is substantial uncertainty inherent in the estimate, much of which cannot

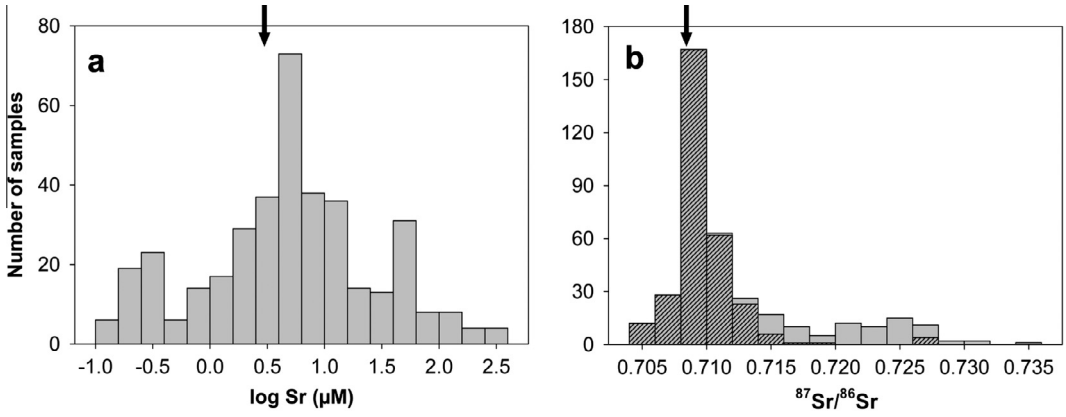

Fig. 5. Frequency distribution of (a) log-transformed Sr concentrations and (b) $^{87}Sr/^{86}Sr$ ratios in global meteoric groundwaters ($n = 381$). Light-colored bars in (b) highlight samples from the unusually radiogenic Ganges–Brahmaputra region. Arrows indicate the flow-weighted global average groundwater composition based on the lithological model (2.9 μM Sr and $^{87}Sr/^{86}Sr$ of 0.7089). Data compiled from the current work and literature references cited in Fig. 4.

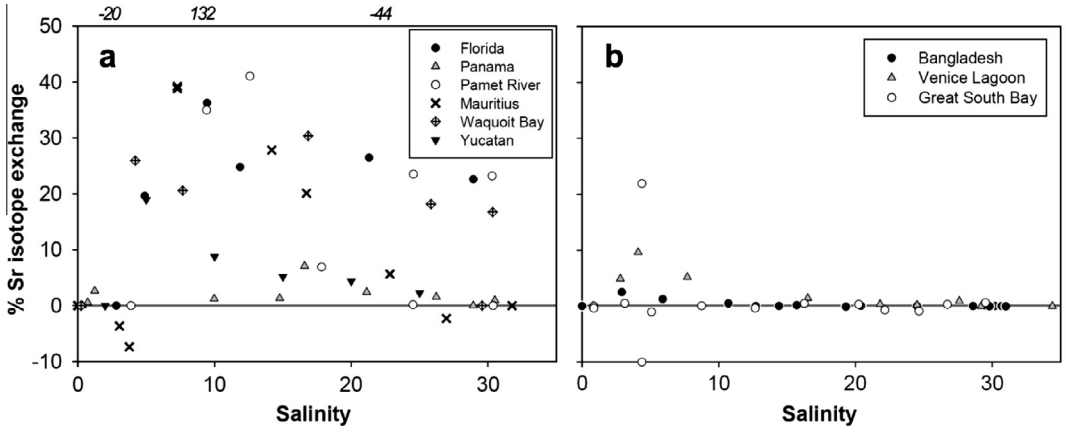

Fig. 6. Relative proportion of $^{87}Sr/^{86}Sr$ isotope exchange in (a) subterranean and (b) surface estuaries. Positive numbers indicate that isotope exchange results a $^{87}Sr/^{86}Sr$ signature more similar to the groundwater end-member than seawater. Three out-of-range values calculated for Mauritius, Florida, and Waquoit Bay STE sites are indicated at their appropriate salinity along the top of (a).

be evaluated at this time. For example, we use an estimate of meteoric SGD for which no associated uncertainties were reported (Zektser et al., 2006). This makes it difficult to quantitatively evaluate the accuracy of the calculated SGD Sr flux, and some caution is warranted when viewing the results. Sources and likely magnitudes of uncertainty in the model estimate are discussed in detail in Section 4.4.3.

The volumetric discharge of meteoric groundwater was taken from the regionally-delineated hydrogeologic assessment of Zektser et al. (2006). Global meteoric SGD total 2397 $km^3\ y^{-1}$, which is approximately 6% of the estimated global river discharge (38,900 $km^3\ y^{-1}$; Peucker-Ehrenbrink et al., 2010). The estimate of Zektser et al. (2006) is probably slightly low, and an SGD volume twice as large would be easily within the range of other estimates (up to 20% of river discharge; summarized by Burnett et al., 2003). It is assumed here that the relative geographic patterns of SGD hold, even if total volumetric discharge is revised upward.

Groundwater Sr concentrations and ratios correlate with aquifer lithology (McNutt, 2000), although incongruent weathering causes $^{87}Sr/^{86}Sr$ of groundwater to differ from that of aquifer lithology (e.g., Franklyn et al., 1991). The SGD end-member Sr composition can therefore be estimated from continental coastal geology using the Sr content and $^{87}Sr/^{86}Sr$ isotope composition of groundwaters reported for aquifers of various lithologies. Coastal aquifer lithologies were estimated using the coarse ($2° \times 2°$) global map of Gibbs and Kump (1994) that is based on the paleolithologic maps of Ronov (1989). Groundwater Sr composition was approximated according to patterns reported in the literature (see Fig. 4) for each of the six lithologic classes listed by Gibbs and Kump (1994): carbonates, shales, sandstones, igneous, shields, and complex lithology (Table 4). For this last category, mixed-composition aquifers were assumed to primarily reflect solution of even minor carbonate components (McNutt, 2000). The end-member Sr concentration

and $^{87}Sr/^{86}Sr$ composition for this category were estimated arbitrarily, but conservatively, to have intermediate Sr concentrations (2 μM) and $^{87}Sr/^{86}Sr$ slightly less radiogenic (0.7090) than modern seawater. If the composition were actually equal parts of the other five lithological categories, it would more closely resemble the carbonate end-member (3.5 μM, $^{87}Sr/^{86}Sr = 0.7086$). Thus, our estimate is conservative, and global SGD may represent a greater Sr mass flux that is less radiogenic than calculated below. An additional category was added to account for the potential Sr-rich, very radiogenic groundwater of the Ganges–Brahmaputra region. Given the low resolution of the lithology map, different rock types were assigned equal importance in the SGD regions in which they were present (see Supporting information, Table S1). Average groundwater composition based on lithology was estimated for each SGD region outlined by Zektser et al. (2006).

The estimated Sr mass flux is $7.1–14 \times 10^9$ mol y^{-1} (this range derives from the assumption that the Zektser et al., 2006, estimate may be low by a factor of two; e.g., Burnett et al., 2003), with an average, discharge and concentration-weighted SGD end-member composition of 2.9 μM Sr and $^{87}Sr/^{86}Sr$ of 0.7089 (Table S1). This average groundwater Sr concentration is somewhat lower than indicated by groundwater data compiled from available literature, which indicates a median value slightly above 5 μM (Fig. 5a). This suggests that the groundwater Sr input estimated here may under-represent Sr-rich sources such as carbonates, which are less radiogenic than other sources. Conversely, it may reflect the fact that regions with lower groundwater Sr concentrations are globally more important in our model (Table 4). The groundwater end-member Sr isotope ratio is consistent with the literature data, which have a median $^{87}Sr/^{86}Sr$ value of approximately 0.709 (Fig. 5b). Because karsts and volcanic aquifers are especially permeable, the average flow-weighted groundwater end-member reflects a greater contribution of less-radiogenic Sr.

Using 0.7089 as the end-member $^{87}Sr/^{86}Sr$ value for an SGD Sr flux of 7.1×10^9 mol y^{-1}, SGD accounts for a minimum 2% of the marine $^{87}Sr/^{86}Sr$ budget (Table 3). As discussed above, values used here for SGD volume flux and end-member Sr concentration may each be a factor of 2 or more too low, and SGD may represent as much as 8% of the global marine Sr budget. Clearly, SGD is a significant component of the marine Sr isotope budget, and has been largely overlooked in most, but not all (Chaudhuri and Clauer, 1986; Basu et al., 2001; Allègre et al., 2010) previous mass balance estimates. However, if the marine Sr isotope budget is currently at steady state, a major flux of relatively non-radiogenic Sr remains unaccounted for. Island arcs probably contribute significantly to this flux (Fiege et al., 2010; Allègre et al., 2010), although Sr concentrations (~0.4 μM) and isotope ratios (>0.704) in waters from these sources are unlikely to fully account for the deficit, and subaerial contributions (rivers) from such areas are included in the river end-member values we use in this study (Peucker-Ehrenbrink et al., 2010).

4.4.2. Brackish SGD-driven Sr flux – Isotope exchange in the STE

Non-conservative behavior of $^{87}Sr/^{86}Sr$ was observed in five of the six subterranean estuaries sampled (Fig. 6a), not including the shallow-aquifer GSB and Venice sites where mixing patterns indicated unusual Sr sources (probably sea salt aerosol from shallow groundwater recharge). Isotope exchange appears responsible for the observed non-conservative behavior because Sr concentrations mixed conservatively in the STE at these five sites. Furthermore, at all five sites, mixing patterns indicated that isotope exchange resulted in input of Sr that resembled the meteoric groundwater end-member. The extent of this exchange was evaluated with data from the five STE sites exhibiting non-conservative patterns. The fraction of groundwater-derived Sr in an STE sample can be estimated as

$$f = \frac{R_{STE} - R_{SW}}{R_{GW} - R_{SW}} \quad (2)$$

where R is the $^{87}Sr/^{86}Sr$ isotope ratio, and subscripts SW, GW, and STE denote seawater end-member, groundwater end-member, and intermediate-salinity samples from the subterranean estuary, respectively. The difference of this groundwater-derived Sr and that expected from conservative mixing between meteoric groundwater and seawater end-members reflects the isotope exchange required to cause the observed non-conservative behavior. At the five sites, isotope exchange ranged from 0–40%, and was greatest in the salinity range of 5–15 (Fig. 6a). Panama was the only site that exhibited minimal non-conservative mixing of Sr isotope ratios in the STE (maximum 7% isotope exchange). Similar treatment of the data from the three surface estuaries (Bangladesh, Venice, and GSB) demonstrates that there was limited (<10%) or no isotope exchange in these surface systems (Fig. 6b). However, the five STE sites that did exhibit non-conservative mixing of Sr isotopes represent a wide range of lithologies – carbonate (Florida and Yucatan), basaltic/volcanic island (Mauritius), and granitic glacial till (Pamet River and Waquoit Bay) – indicating that such exchange processes are not limited to specific aquifer types.

Numerous studies have concluded that SGD comprises a substantial fraction of recirculated seawater (i.e., seawater mixing in the STE), and meteoric groundwater usually accounts for some 10% of the total discharge (Moore, 2010). Assuming a salinity of 30 for coastal seawater, brackish SGD should have a salinity of approximately 27 (total SGD comprises ~10% meteoric groundwater). The volume of global brackish SGD can be estimated from the meteoric discharge, and is on the order of $2–5 \times 10^{16}$ L y^{-1}. Moore et al. (2008) estimate an SGD flux of $2–4 \times 10^{16}$ L y^{-1} for the Atlantic Ocean alone, although much of this SGD flux occurs on the continental shelf and is not influenced by meteoric groundwater discharge. We consider our estimate of brackish SGD as very conservative because our estimate of global SGD is lower than other, reliable estimates for the Atlantic Ocean basin alone.

The mass of Sr that undergoes isotope exchange in the STE is a fraction of the total Sr in brackish groundwater. The greatest isotope exchange was observed at a salinity of 10 ± 2 (Fig. 6a), corresponding to a Sr concentration of $\sim 28 \pm 5$ μM. Based on the total brackish SGD volume flux discussed above (at salinity 27), this constitutes a fractional SGD flux of 7–11 $\times 10^{15}$ L y^{-1}. Assuming that this Sr has undergone ~25% isotope exchange (Fig. 6a), SGD includes a Sr flux of 16–35 $\times 10^{10}$ mol y^{-1} with an isotope ratio of 0.7091. This is a fraction of the total brackish SGD, and represents only the Sr that has undergone isotope exchange. Assuming there is limited or no further isotope exchange as more seawater mixing occurs, the total discharge at salinity 27 will have a higher Sr concentration and a ratio more similar to seawater. The effect of the fractional and total brackish SGD flux on the isotope budget would be the same. The brackish flux that has been modified by isotope exchange in the STE can balance an additional 11–23% of the radiogenic river Sr input (Table 3). Note that the brackish SGD flux calculated here refers to seawater Sr that has undergone isotope exchange in the subterranean estuary, and is different from the meteoric groundwater Sr that was discussed in Section 4.4.1. While isotope exchange affects the isotopic composition of saline groundwater (i.e., recirculated seawater), it does not appear to alter the concentration of dissolved Sr. Thus, the saline component of the brackish SGD flux is not a net source of dissolved Sr to the ocean.

4.4.3. Uncertainties in the SGD source term

Together, fresh and brackish SGD can account for 13–31% of the oceanic Sr isotope budget (Table 3). This is comparable to, or greater than the diagenetic and hydrothermal terms. Although our estimate of the less-radiogenic Sr input by SGD does not appear to be sufficient to balance the radiogenic river source, it substantially reduces the imbalance. The magnitude and chemical composition of SGD are poorly known, and this source term may well be increased as the phenomenon becomes better understood.

There remain a number of significant sources of uncertainty in the SGD-driven Sr flux that are too poorly constrained to reliably evaluate uncertainty on the overall SGD Sr source term. The most fundamental uncertainty in this flux is associated with the volumetric discharge of water (e.g., Burnett et al., 2003). Because our global model relies on spatial delineation of SGD inputs, accurate and detailed hydrologic models (e.g., PCR-GLOBWB; van Beek and Bierkens, 2008) and SGD typologies (e.g., Bokuniewicz et al., 2003) can help constrain the distribution and magnitude of global SGD patterns. Estimates of SGD-driven Sr flux will also benefit from coupling with high-resolution coastal lithology maps (e.g., Dürr et al., 2005). In our assessment, the SGD volume flux is made up of approximately equal parts from aquifers of the five major lithology types (11–17%; Table 4), and a contribution about twice that size (32%) from the "complex" lithology due to the higher prevalence of this type in the lithology map. This estimate considers variations in recharge and hydraulic head, but the similarity of SGD flux from these different aquifer types is suspect considering the ~11 orders-of-magnitude variation in permeability for different aquifer lithologies (Gleeson et al., 2011). Explicitly integrated lithology-discharge models will be an invaluable tool for evaluating the SGD source of Sr and other chemical constituents to the global ocean.

Estimates of SGD-driven Sr input to the ocean also will be improved by using empirical data to define local end-members. This is especially important for the carbonate end-member, which has a disproportionate effect on the global average due to a high Sr concentration and a $^{87}Sr/^{86}Sr$ less radiogenic than present-day seawater (Table 4). In the current model, varying the carbonate end-member Sr concentration between 5 and 15 μM results in a global flux estimate that ranges from 0.6 to 0.8 $\times 10^{10}$ mol Sr y^{-1}. Similarly, varying the carbonate end-member $^{87}Sr/^{86}Sr$ ratio between 0.707 and 0.709 across the same 5–15 μM concentration range gives a global average SGD $^{87}Sr/^{86}Sr$ ratio that varies from 0.7083 to 0.7094.

Qualitative evaluation of uncertainties introduced by different components of the global model can be made using Table 4. The primary controls (62% of the flux) on the meteoric SGD-driven Sr flux are the carbonate and "complex"-lithology sources. These sources dominate due to the high Sr concentration of the carbonate end-member (10 μM), and the large volume flux associated with the "complex" end-member (32% of the global flux). Not surprisingly, the granite lithology source contributes only a minor fraction (2%) of the global Sr mass flux due to the low Sr concentrations assigned in the model to this end-member (0.5 μM). The Ganges–Brahmaputra source has a high end-member Sr concentration (6 μM), but represents only 3% of the global Sr flux due to its small volume flux. For the global SGD $^{87}Sr/^{86}Sr$ isotope ratio, groundwater sources that are radiogenic relative to seawater have a positive effect on the SGD isotope ratio, while those that are non-radiogenic relative to seawater have a negative effect on the SGD isotope ratio. Consequently, the "complex" lithology, which has an $^{87}Sr/^{86}Sr$ isotope ratio that is similar to seawater (0.7090), contributes ~4% of the less radiogenic flux and barely affects the $^{87}Sr/^{86}Sr$ of the global SGD Sr end-member. Conversely, the carbonate, igneous, and Ganges–Brahmaputra end-members all have major impact on the $^{87}Sr/^{86}Sr$ composition of global SGD because their compositions are so different from seawater (Table 4).

In addition to the global flux of meteoric SGD, the model input for end-member $^{87}Sr/^{86}Sr$ isotope ratios, Sr concentrations, and flux apportionment (first three columns in Table 4) all have an effect on the final estimate of SGD-driven Sr flux and its uncertainty. Our global estimate of an SGD Sr source that is slightly less radiogenic than modern seawater is likely to be conservative considering that the carbonate end-member Sr concentration could be much higher, and that of the granite end-member lower, than used in our model (e.g., Fig. 5). The Ganges–Brahmaputra SGD source could also be less important than the model suggests (see Section 4.3). In concert, these effects would lead to a global-average SGD source of Sr that is even less radiogenic than we propose, suggesting that reducing uncertainty in our model would tend to strengthen our conclusions. Clearly, refining the groundwater end-member,

and particularly that of carbonate aquifers, is necessary to accurately constrain the global SGD Sr source. Such refinement is particularly important given that the brackish SGD source varies with the meteoric SGD end-member.

Information is lacking from several major SGD sources because most SGD work has been performed in the northern hemisphere. For example, we are not aware of any data on SGD for Papua New Guinea, the west coast of South America, or West Africa, which represent a combined 26% of global meteoric SGD (Table S1; Zektser et al., 2006). Fiege et al. (2009) report an average, flux-weighted $^{87}Sr/^{86}Sr$ value of 0.7057 in rivers draining Chile into the Pacific, indicating that this region may also constitute a SGD source of Sr that is less radiogenic than seawater. A large and isotopically-distinct SGD flux from western South America would be an important component of the global budget that is not captured in our current assessment (currently, 0.7090; Table S1). As well, many ocean islands are not included in the SGD estimate used here, and these may represent a major source of SGD and non-radiogenic Sr to the ocean (Zektser et al., 2006; Allègre et al., 2010). It is also not entirely clear how significant the Ganges–Brahmaputra region is in delivering very radiogenic Sr to the ocean. There is some controversy regarding SGD from this coastline (Harvey, 2002; Basu et al., 2002), and our data from the Bay of Bengal do not show evidence for an SGD source of radiogenic Sr. Lastly, it will be important to determine if isotope exchange in the STE always favors the groundwater end-member, as is apparent from the present study. Some evidence from surface estuaries suggests that isotope exchange is alternately a source of groundwater or marine Sr, depending on recharge–discharge characteristics (Rahaman and Singh, 2012).

5. CONCLUSIONS

The Sr flux to the ocean from SGD is a major component (13–31%) of the marine Sr isotope budget. Groundwater input with a $^{87}Sr/^{86}Sr$ less radiogenic than seawater buffers the rise in the $^{87}Sr/^{86}Sr$ of seawater caused by the fluvial input of radiogenic Sr, and is comparable in magnitude to the flux driven by submarine hydrothermal circulation through oceanic spreading centers. Our assessment implies that the modern oceanic Sr budget is likely not balanced.

The fact that the SGD-driven Sr flux is a major component of the budget implies that changes in SGD volume inputs over geologic time may have contributed to observed temporal variations in marine $^{87}Sr/^{86}Sr$ ratios. Indeed, rivers and SGD are the only components of the Sr budget that are likely to have varied significantly over the past tens of millions of years (e.g., Cogné and Humler, 2006, for variations in ocean crust production rates). River and SGD Sr sources have likely had – at least for the last few million years – opposite impacts on the oceanic Sr ratio, and periods of rapid or slow change in the oceanic ratio may indicate variation in the relative importance of these two inputs.

However, the mass balance presented here is based on observed trends in modern subterranean estuaries and does not allow estimates of the effects of non-steady state in SGD fluxes and the marine Sr budget that might arise from continental breakup or agglomeration (Chaudhuri and Clauer, 1986), glacial-interglacial sea level changes (Milliman, 1993), or from rapid natural and anthropogenic seawater intrusion into coastal aquifers (e.g., Jørgensen et al., 2008).

Finally, the conservative behavior of Sr concentrations in the subterranean estuary demonstrated here should simplify exercises to refine the meteoric SGD component of the marine Sr budget. However, isotope exchange in the subterranean estuary makes brackish SGD an important contributor to the Sr isotope budget. Similar SGD isotope exchange has been inferred from Sr isotope data in surficial estuaries (Rahaman and Singh, 2012), highlighting the global importance of this process. Scaling this exchange to the global ocean is a difficult and uncertain task that will require future STE studies at more diverse locations worldwide. It is clear from this and other studies (Basu et al., 2001; Allègre et al., 2010) that the global SGD-driven Sr flux cannot necessarily be simply considered some fraction of the average river input to the ocean (Gruszczynski et al., 1992; Veizer, 1989). Given the coherent patterns observed for different aquifer lithologies, and the conservative mixing behavior of Sr concentrations in the STE, adapting a typological SGD model (e.g., Bokuniewicz, 2001; Bokuniewicz et al., 2003) may help to better constrain the global SGD Sr source. Similar efforts to identify and categorize different STE types will help connect different physical systems with geochemical processes, which will be critical for extrapolating STE influences to a global scale. However, until we better understand global patterns in coastal groundwater discharge and – especially – are able to separate meteoric and marine groundwater components in groundwater flux estimates, Sr input from SGD will remain an important but not adequately constrained component of the global ocean Sr budget.

ACKNOWLEDGMENTS

Billy Moore graciously provided the Ganges–Brahmaputra samples. We thank Jerzy Blusztajn for assistance performing MC-ICPMS analyses in the WHOI ICPMS Facility and guidance with post-processing. We also thank Laura Robinson for providing clean lab access for sample processing. This paper benefitted from thoughtful and detailed reviews by W. Rahaman and two anonymous reviewers. This project was supported by funding from the WHOI Coastal Ocean Institute and the Tropical Research Initiative, and NSF OCE-0751525 to M.A.C. B.P.E. acknowledges financial support from NSF ETBC-85101500 and a WHOI Coastal Ocean Institute Fellowship. This is contribution number 1415 from the School of Marine & Atmospheric Sciences (Stony Brook University).

APPENDIX A. SUPPLEMENTARY DATA

Supplementary data associated with this article can be found, in the online version, at http://dx.doi.org/10.1016/j.gca.2013.03.021.

REFERENCES

Alam M., Alam M. M., Curray J. R., Chowdhury A. L. R. and Gani M. R. (2003) An overview of the sedimentary geology of the Bengal Basin in relation to the regional tectonic framework and basin-fill history. *Sed. Geol.* **155**, 179–208.

Albarede F., Michard A., Minster J. F. and Michard G. (1981) $^{87}Sr/^{86}Sr$ ratios in hydrothermal waters and deposits from the East Pacific Rise at 21 N. *Earth Planet. Sci. Lett.* **55**, 229–236.

Allègre C. J., Louvat P., Gaillardet J., Meynadier L., Rad S. and Capmas F. (2010) The fundamental role of island arc weathering in the oceanic Sr isotope budget. *Earth Planet. Sci. Lett.* **292**, 51–56.

Andersson P. S., Wasserburg G. J., Ingri J. and Stordal M. C. (1994) Strontium, dissolved and particulate loads in fresh and brackish waters: The Baltic Sea and Mississippi Delta. *Earth Planet. Sci. Lett.* **124**, 195–210.

Basu A. R., Jacobsen S. B., Poreda R. J., Dowling C. B. and Aggarwal P. K. (2001) Large groundwater strontium flux to the oceans from the Bengal Basin and the marine strontium isotope record. *Science* **293**, 1470–1473.

Basu A. R., Jacobsen S. B., Poreda R. J., Dowling C. B. and Aggarwal P. K. (2002) Reply to Harvey. *Science* **296**, 1563A.

Bau M., Alexander B., Chesley J. T., Dulski P. and Brantley S. L. (2004) Mineral dissolution in the Cape Cod aquifer, Massachusetts, USA: I. Reaction stoichiometry and impact of accessory feldspar and glauconite on strontium isotopes, solute concentrations, and REY distribution. *Geochim. Cosmochim. Acta* **68**(6), 1199–1216.

Beck, A. J. (2007) Submarine groundwater discharge (SGD) and dissolved trace metal cycling in the subterranean estuary and coastal ocean. Ph. D. dissertation. Stony Brook Univ. 308pp.

Beck A. J., Cochran J. K. and Sanudo-Wilhelmy S. A. (2010) The distribution and speciation of dissolved trace metals in a shallow subterranean estuary. *Mar. Chem.* **121**, 145–156.

Blum J. D., Gazis C. A., Jacobson A. D. and Page Chamberlain C. (1998) Carbonate versus silicate weathering in the Raikhot watershed within the High Himalayan Crystalline Series. *Geology* **26**, 411–414.

Böhlke J. K. and Horan M. (2000) Strontium isotope geochemistry of groundwaters and streams affected by agriculture, Locust Grove, MD. *Appl. Geochem.* **15**, 599–609.

Bokuniewicz H. (2001) Toward a coastal ground-water typology. *J. Sea Res.* **46**(2), 99–108.

Bokuniewicz H., Buddemeier R., Maxwell B. and Smith C. (2003) The typological approach to submarine groundwater discharge (SGD). *Biogeochemistry* **66**(1–2), 145–158.

Bouchaou L., Michelot J. L., Vengosh A., Hsissou Y., Qurtobi M., Gaye C. B., Bullen T. D. and Zuppi G. M. (2008) Application of multiple isotopic and geochemical tracers for investigation of recharge, salinization, and residence time of water in the Souss–Massa aquifer, southwest of Morocco. *J. Hydrol.* **352**, 267–287.

Brambati A., Carbognin L., Quaia T., Teatini P. and Tosi L. (2003) The Lagoon of Venice: Geological setting, evolution and land subsidence. *Episodes* **26**, 264–268.

Brammer, H., Antoine, J., Kassam, A. H. and van Venthuizen, H. T. (1988) Land resources appraisal of Bangladesh for agricultural development. Report 5: Land Resources. BGD/81/035. United Nations Development Programme, Food and Agriculture Organization. 122pp.

Burnett W. C., Bokuniewicz H. J., Huettel M., Moore W. S. and Taniguchi M. (2003) Groundwater and pore water inputs to the coastal zone. *Biogeochemistry* **66**, 3–33.

Burnett W. C., Aggarwal P. K., Aureli A., Bokuniewicz H., Cable J. E., Charette M. A., Kontar E., Krupa S., Kulkarni K. M., Loveless A., Moore W. S., Oberdorfer J. A., Oliveira J., Ozyurt N., Povinec P., Privitera A. M. G., Rajar R., Ramassur R. T., Scholten J., Stieglitz T., Taniguchi M. and Turner J. V. (2006) Quantifying submarine groundwater discharge in the coastal zone via multiple methods. *Sci. Total Environ.* **367**, 498–543.

Cambareri T. C. and Eichner E. M. (1998) Watershed delineation and ground water discharge to a coastal embayment. *Ground Water* **36**, 626–634.

Capo R. C. and DePaolo D. J. (1990) Seawater strontium isotopic variations from 2.5 million years ago to the present. *Science* **249**(4964), 51–55.

Carroll J., Falkner K. K., Brown E. T. and Moore W. S. (1993) The role of the Ganges–Brahmaputra mixing zone in supplying barium and 226Ra to the Bay of Bengal. *Geochim. Cosmochim. Acta* **57**, 2981–2990.

Cartwright I., Weaver T. and Petrides B. (2007) Controls on $^{87}Sr/^{86}Sr$ ratios of groundwater in silicate-dominated aquifers: SE Murray Basin, Australia. *Chem. Geol.* **246**, 107–123.

Charette M. A. (2007) Hydrologic forcing of submarine groundwater discharge: Insight from a seasonal study of radium isotopes in a groundwater-dominated salt marsh estuary. *Limnol. Oceanogr.* **52**, 230–239.

Charette M. A. and Sholkovitz E. R. (2002) Oxidative precipitation of groundwater derived ferrous iron in the subterranean estuary of a coastal bay. *Geophys. Res. Lett.* **29**(10). http://dx.doi.org/10.1029/2001GL014512.

Charette M. A. and Allen M. C. (2006) Precision groundwater sampling in coastal aquifers using a direct push shielded screen well-point system. *Groundwater Monit. Rem.* **26**(2), 87–93.

Charette M. A. and Sholkovitz E. R. (2006) Trace element cycling in a subterranean estuary: Part 2. Geochemistry of the pore water. *Geochim. Cosmochim. Acta* **70**(4), 811–826.

Charette M. A. and Smith W. H. F. (2010) The volume of Earth's ocean. *Oceanography* **23**, 104–106.

Charette M. A., Sholkovitz E. R. and Hansel C. M. (2005) Trace element cycling in a subterranean estuary: Part 1. Geochemistry of the permeable sediments. *Geochim. Cosmochim. Acta* **69**(8), 2095–2109.

Charette, M. A., Gonneea, M. E., Henderson, P. B., Rao, A. and Herrera-Silveira, J. (2008) Trace metal biogeochemistry in Karstic Subterranean Estuaries. In *AGU/ASLO Ocean Sciences Meeting*, Orlando, Florida.

Chaudhuri S. and Clauer N. (1986) Fractionations of isotopic composition of strontium in seawater during the Phaerozoic Eon. *Chem. Geol. (Isotope Geoscience Section)* **59**, 293–303.

Coates A. G., Collins L. S., Aubry M. P. and Berggren W. A. (2004) The geology of the Darien, Panama, and the late Miocene–Pliocene collision of the Panama arc with northwestern South America. *Geol. Soc. Am. Bull.* **116**, 1327–1344.

Cochran J. K., Landman N. H., Turekian K. K., Michard A. and Schrag D. P. (2003) Paleoceanography of the Late Cretaceous (Maastrichtian) Western Interior Seaway of North America: Evidence from Sr and O isotopes. *Palaeogeogr. Palaeoclimatol. Palaeoecol.* **191**, 45–64.

Cogné J.-P. and Humler E. (2006) Trends and rhythms in global seafloor generation rate. *Geochem. Geophys. Geosyst.* **7**(3). http://dx.doi.org/10.1029/2005GC001148.

Coleman J. M. (1969) Brahmaputra river: Channel processes and sedimentation. *Sediment. Geol.* **3**, 129–239.

Davis A. C., Bickle M. J. and Teagle D. A. H. (2003) Imbalance in the oceanic strontium budget. *Earth Planet. Sci. Lett.* **211**, 173–187.

de Villiers S. (1999) Seawater strontium and Sr/Ca variability in the Atlantic and Pacific oceans. *Earth Planet. Sci. Lett.* **171**, 623–634.

Dowling C. B., Poreda R. J. and Basu A. R. (2003) The groundwater geochemistry of the Bengal Basin: Weathering,

chemsorption, and trace metal flux to the oceans. *Geochim. Cosmochim. Acta* **67**(12), 2117–2136.

Dürr H. H., Meybeck M. and Dürr S. (2005) Lithologic composition of the Earth's continental surfaces derived from a new digital map emphasizing riverine material transfer. *Global Biogeochem. Cycles* **19**, GB4S10. http://dx.doi.org/10.1029/2005GB002515.

Edmond J. M. (1992) Himalayan tectonics, weathering processes, and the strontium isotope record in marine limestones. *Science* **258**(5088), 1594–1597.

Elderfield H. and Gieskes J. M. (1982) Sr isotope in interstitial waters of marine sediments from Deep Sea Drilling Project cores. *Nature* **300**, 493–497.

Elderfield H. and Greaves M. J. (1981) Strontium isotope geochemistry of Icelandic geothermal systems and implications for sea-water chemistry. *Geochim. Cosmochim. Acta* **45**(11), 2201–2212.

Farrell J. W., Clemens S. C. and Gromet L. P. (1995) Improved chronostratigraphic reference curve of late Neogene seawater $^{87}Sr/^{86}Sr$. *Geology* **23**, 403–406.

Fiege K., Miller C. A., Robinson L. F., Figueroa R. and Peucker-Ehrenbrink B. (2009) Strontium isotopes in Chilean rivers: The flux of unradiogenic continental Sr to seawater. *Chem. Geol.* **268**, 337–343.

Ford D. and Williams P. (2007) *Karst Hydrogeology and Geomorphology*. John Wiley and Sons, West Sussex, 562pp.

Frost C. D., Pearson B. N., Ogle K. M., Heffern E. L. and Lyman R. M. (2002) Sr isotopic tracing of aquifer interactions in an area of coal and methane production, Powder River Basin, Wyoming. *Geology* **30**, 923–926.

Frost C. D. and Toner R. N. (2004) Strontium isotopic identification of water–rock interaction and groundwater mixing. *Ground Water* **42**, 418–432.

Galy A., France-Lanord C. and Derry L. A. (1999) The strontium isotopic budget of Himalayan rivers in Nepal and Bangladesh. *Geochim. Cosmochim. Acta* **63**, 1905–1925.

Garcia-Solsona E., Masqué P., Garcia-Orellana J., Rapaglia J. P., Beck A. J., Cochran J. K., Bokuniewicz H., Zaggia L. and Collavini F. (2008) Estimating submarine groundwater discharge Isola La Cura, northern Venice Lagoon (Italy), by using the radium quartet. *Mar. Chem.* **109**, 292–306.

Gibbs M. T. and Kump L. R. (1994) Global chemical erosion during the last glacial maximum and the present: Sensitivity to changes in lithology and hydrology. *Paleoceanography* **9**(4), 529–543.

Gilli A., Hodell D. A., Kamenov G. D. and Brenner M. (2009) Geological and archaeological implications of strontium isotope analysis of exposed bedrock in the Chicxulub crater basin, northwestern Yucatán, Mexico. *Geology* **37**, 723–726.

Gleeson T., Smith L., Moosdorf N., Hartmann J., Dürr H. H., Manning A. H., van Beek L. P. H. and Jellinek A. M. (2011) Mapping permeability over the surface of the Earth. *Geophys. Res. Lett.* **38**(2). http://dx.doi.org/10.1029/2010GL045565.

Gosselin D. C., Harvey F. E., Frost C., Stotler R. and Macfarlane P. A. (2004) Strontium isotope geochemistry of groundwater in the central part of the Dakota (Great Plains) aquifer, USA. *Appl. Geochem.* **19**(2004), 359–377.

Gruszczynski M., Hofftnan A., Malkowski K. and Veizer J. (1992) Seawater strontium isotopic perturbation at the Permian-Triassic boundary, West Spitsbergen, and its implications for the interpretation of strontium isotopic data. *Geology* **20**, 779–782.

Harvey C. F. (2002) Groundwater flow in the Ganges delta. *Science* **296**, 1563.

Helstrup, T. (2006) Environmental isotopic and hydrochemical characteristics of groundwater from the Cretaceous-Eocene limestone aquifer in the Keta Basin, Ghana, and the Coastal Sedimentary Basin of Togo. Ph. D. thesis, February 2006. University of Copenhagen. 93pp.

Henderson G. M., Martel D. J., O'Nions R. K. and Shackleton N. J. (1994) Evolution of seawater $^{87}Sr/^{86}Sr$ over the last 400 ka: The absence of glacial/interglacial cycles. *Earth Planet. Sci. Lett.* **128**, 643–651.

Hess J., Bender M. L. and Schilling J.-G. (1986) Evolution of the ratio of strontium-87 to strontium-86 in seawater from Cretaceous to present. *Science* **231**, 979–984.

Hickey T. D., Hine A. C., Shinn E. A., Kruse S. E. and Poore R. Z. (2010) Pleistocene carbonate stratigraphy of South Florida: Evidence for high-frequency sea-level cyclicity. *J. Coastal Res.* **26**, 605–614.

Hodell D. A., Mueller P. A. and Garrido J. R. (1991) Variations in the strontium isotopic composition of seawater during the Neogene. *Geology* **19**, 24–27.

Holmden C., Papanastassiou D. A., Blanchon P. and Evans S. (2012) Δ44/40Ca variability in shallow water carbonates and the impact of submarine groundwater discharge on Ca-cycling in marine environments. *Geochim. Cosmochim. Acta* **83**, 179–194.

Hogan J. F., Blum J. D., Siegel D. I. and Glaser P. H. (2000) $^{87}Sr/^{86}Sr$ as a tracer of groundwater discharge and precipitation recharge in the Glacial Lake Agassiz Peatlands, Northern Minnesota. *Water Resour. Res.* **36**(12), 3701–3710.

Horwitz E. P., Dietz M. L. and Fisher D. E. (1991) Separation and preconcentration of strontium from biological, environmental, and nuclear waste samples by extraction chromatography using a crown ether. *Anal. Chem.* **63**, 522–525.

Huff, G. F. and Bonck, J. P. (1993) Saltwater in shallow aquifers in east-central and northeastern Louisana and southeastern Arkansas. US Geological Survey Open-File Report 93-494.

Jacobson A. D. and Wasserburg G. J. (2005) Anhydrite and the Sr isotope evolution of groundwater in a carbonate aquifer. *Chem. Geol.* **214**, 331–350.

Jackson M. G. and Hart S. R. (2006) Strontium isotopes in melt inclusions from Samoan basalts: Implications for heterogeneity in the Samoan plume. *Earth Planet. Sci. Lett.* **245**, 260–277.

Johannesson K. H. and Burdige D. J. (2007) Balancing the global oceanic neodymium budget: Evaluating the role of groundwater. *Earth Planet. Sci. Lett.* **253**, 129–142.

Johannesson K. H., Chevis D. A., Burdige D. J., Cable J. E., Martin J. B. and Roy M. (2011) Submarine groundwater discharge is an important net source of light and middle REEs to coastal waters of the Indian River Lagoon, Florida, USA. *Geochim. Cosmochim. Acta* **75**, 825–843.

Jørgensen N. O. and Banoeng-Yakubo B. K. (2001) Environmental isotopes (^{18}O, ^{2}H, and $^{87}Sr/^{86}Sr$) as a tool in groundwater investigations in the Keta Basin, Ghana. *Hydrogeol. J.* **9**, 190–201.

Jørgensen N. O., Andersen M. S. and Engesgaard P. (2008) Investigation of a dynamic seawater intrusion event using strontium isotopes ($^{87}Sr/^{86}Sr$). *J. Hydrol.* **348**, 257–269.

Kim Y., Lee K.-S., Koh D.-C., Dae-Ha Lee, Lee S.-G., Park W.-B., Koh G.-W. and Woo N.-C. (2003) Hydrogeochemical and isotopic evidence of groundwater salinization in a coastal aquifer: A case study in Jeju volcanic island, Korea. *J. Hydrol.* **270**, 282–294.

Klaus J. S., Hansen B. T. and Buapeng S. (2007) $^{87}Sr/^{86}Sr$ ratio: A natural tracer to monitor groundwater flow paths during artificial recharge in the Bangkok area, Thailand. *Hydrogeol. J.* **15**, 745–758.

Krabbenhöft A., Eisenhauer A., Böhm F., Vollstaedt H., Fietzke J., Liebetrau V., Augustin N., Peucker-Ehrenbrink B., Müller M. N., Horn C., Hansen B. T., Nolte N. and Wallmann K.

(2010) Constraining the marine strontium budget with natural strontium isotope fractionations ($^{87}Sr/^{86}Sr^*$, $\delta^{88/86}Sr$) of carbonates, hydrothermal solutions and river waters. *Geochim. Cosmochim. Acta* **74**, 4097–4109.

Krishnaswami S., Trivedi J. R., Sarin M. M., Ramesh R. and Sharma K. K. (1992) Strontium isotopes and rubidium in the Ganga–Brahmaputra river system: Weathering in the Himalaya, fluxes to the Bay of Bengal and contributions to the evolution of oceanic $^{87}Sr/^{86}Sr$. *Earth Planet. Sci. Lett.* **109**, 243–253.

Land M., Ingri J., Andersson P. S. and Öhlander B. (2000) Ba/Sr, Ca/Sr and $^{87}Sr/^{86}Sr$ ratios in soil water and groundwater: Implications for relative contributions to stream water discharge. *Appl. Geochem.* **15**, 311–325.

Li L., Barry A., Stagnitti F. and Parlange J.-Y. (1999) Submarine groundwater discharge and associated chemical input to a coastal sea. *Water Resour. Res.* **35**(11), 3253–3259.

Louvat P. and Allègre C. J. (1998) Riverine erosion rates on Sao Miguel volcanic island, Azores archipelago. *Chem. Geol.* **148**, 177–200.

Franklyn M. T., McNutt R. H., Kamineni D. C., Gascoyne M. and Frape S. K. (1991) Groundwater $^{87}Sr/^{86}Sr$ values in the Eye-Dashwa Lakes pluton, Canada: Evidence for plagioclase-water reaction. *Chem. Geol.* **86**, 111–122.

McNutt R. H. (2000) Strontium isotopes. In *Environmental Tracers in Subsurface Hydrology* (eds. P. G. Cook and A. L. Herczeg). Kluwer, The Netherlands, pp. 233–260.

McNutt R. H., Gascoyne M. and Kamineni (1987) $^{87}Sr/^{86}Sr$ values in groundwaters of the East Bull Lake pluton, Ontario, Canada. *Appl. Geochem.* **2**, 93–101.

Milliman J. D. (1993) Production and accumulation of calcium carbonate in the ocean: Budget of a nonsteady state. *Global Biogeochem. Cycles* **7**(4), 927–957.

Möller P., Weise S. M., Tesmer M., Dulski P., Pekdeger A., Bayer U. and Magri F. (2008) Salinization of groundwater in the North German Basin: Results from conjoint investigation of major, trace element and multi-isotope distribution. *Int. J. Earth Sci.* **97**, 1057–1073.

Moore W. S. (1996) Large groundwater inputs to coastal waters revealed by Ra-226 enrichments. *Nature* **380**(6575), 612–614.

Moore W. S. (1997) High fluxes of radium and barium from the mouth of the Ganges–Brahmaputra river during low river discharge suggest a large groundwater source. *Earth Planet. Sci. Lett.* **150**(1–2), 141–150.

Moore W. S. (1999) The subterranean estuary: A reaction zone of ground water and sea water. *Mar. Chem.* **65**(1–2), 111–125.

Moore W. S. (2010) A reevaluation of submarine groundwater discharge along the southeastern coast of North America. *Global Biogeochem. Cycles* **24**, GB4005. http://dx.doi.org/10.1029/2009GB003747.

Moore W. S. and Shaw T. J. (2008) Fluxes and behavior of radium isotopes, barium, and uranium in seven Southeastern US rivers and estuaries. *Mar. Chem.* **108**, 236–254.

Moore W. S., Sarmiento J. L. and Key R. M. (2008) Submarine groundwater discharge revealed by ^{228}Ra distribution in the upper Atlantic Ocean. *Nat. Geosci.* **1**, 309–311.

Mulligan A. E. and Charette M. A. (2006) Intercomparison of submarine groundwater discharge estimates from a sandy unconfined aquifer. *J. Hydrol.* **327**, 411–425.

Négrel P. (1999) Geochemical study of a granitic area – The Margeride Mountains, France: Chemical element behavior and $^{87}Sr/^{86}Sr$ constraints. *Aquat. Geochem.* **5**, 125–165.

Négrel P. and Deschamps P. (1996) Natural and anthropogenic budgets of a small watershed in the Massif Central (France): Chemical and strontium isotopic characterization in water and sediments. *Aquat. Geochem.* **2**, 1–27.

Nohda S., Kaneoka I., Hanyu T., Xu S. and Uto K. (2005) Systematic variation of Sr-, Nd- and Pb-isotopes with time in lavas of Mauritius, Reunion hotspot. *J. Petrol.* **46**, 505–522.

Palmer M. R. and Edmond J. M. (1989) The strontium isotope budget of the modern ocean. *Earth Planet. Sci. Lett.* **92**(1), 11–26.

Paytan A., Kastner M., Martin E. E., Macdougall J. D. and Herbert T. (1993) Marine barite as a monitor of seawater strontium isotope composition. *Nature* **366**, 445–449.

Perry E., Velazquez-Oliman G. and Marin L. (2002) The hydrogeochemistry of the Karst Aquifer System of the Northern Yucatan Peninsula, Mexico. *Int. Geol. Rev.* **44**, 191–221.

Perry E., Paytan A., Pedersen B. and Velazquez-Oliman G. (2009) Groundwater geochemistry of the Yucatan Peninsula, Mexico: Constraints on stratigraphy and hydrogeology. *J. Hydrol.* **367**, 27–40.

Petelet-Giraud E., Klaver G. and Negrel P. (2009) Natural versus anthropogenic sources in the surface- and groundwater dissolved load of the Dommel river (Meuse basin): Constraints by boron and strontium isotopes and gadolinium anomaly. *J. Hydrol.* **369**, 336–349.

Peucker-Ehrenbrink B., Miller M. W., Arsouze T. and Jeandel C. (2010) Continental bedrock and riverine fluxes of strontium and neodymium isotopes to the oceans. *Geochem. Geophys. Geosyst.* **11**, Q03016. http://dx.doi.org/10.1029/2009GC002869.

Pin C. and Bassin C. (1992) Evaluation of a strontium-specific extraction chromatographic method for isotopic analysis in geological materials. *Anal. Chim. Acta* **269**, 249–255.

Pin C., Briot D., Bassin C. and Poitrasson F. (1994) Concomitant separation of strontium and samarium–neodymium for isotopic analysis in silicate samples, based on specific extraction chromatography. *Anal. Chim. Acta* **298**, 209–217.

Rad S. D., Allègre C. J. and Louvat P. (2007) Hidden erosion on volcanic islands. *Earth Planet. Sci. Lett.* **262**, 109–124.

Rahaman W. and Singh S. K. (2012) Sr and $^{87}Sr/^{86}Sr$ in estuaries of western India: Impact of submarine groundwater discharge. *Geochim. Cosmochim. Acta* **85**, 275–288.

Rahaman W., Singh S. K., Sinha R. and Tandon S. K. (2011) Sr, C and O isotopes in carbonate nodules from the Ganga Plain: Evidence for recent abrupt rise in dissolved $^{87}Sr/^{86}Sr$ ratios of the Ganga. *Chem. Geol.* **285**, 184–193.

Raiber M., Webb J. A. and Bennetts D. A. (2009) Strontium isotopes as tracers to delineate aquifer interactions and the influence of rainfall in the basalt plains of southeastern Australia. *J. Hydrol.* **367**, 188–199.

Rapaglia J. (2005) Submarine groundwater discharge into Venice Lagoon, Italy. *Estuaries* **28**(5), 705–713.

Rapaglia J., Di Sipio E., Bokuniewicz H., Zuppi G. M., Zaggia L., Galgaro A. and Beck A. (2010) Groundwater connections under a barrier beach: A case study in the Venice Lagoon. *Cont. Shelf Res.* **30**, 119–126.

Ronov A. B. (1989) Atlas of Lithological–Paleogeographical Maps of the World: Mesozoic and Cenozoic of Continents and Oceans (eds. V. L. Barsukov and N. P. Laviorov). Nauka, Moscow, 79pp.

Shand P., Darbyshire D. P. F., Love A. J. and Edmunds W. M. (2009) Sr isotope in natural waters: Applications to source characterization and water–rock interaction in contrasting landscapes. *Appl. Geochem.* **24**, 574–586.

Shaw T. J., Moore W. S., Kloepfer J. and Sochaski M. (1998) The flux of barium to the coastal waters of the southeastern United States: The importance of submarine groundwater discharge. *Geochim. Cosmochim. Acta* **62**, 1277–1283.

Siegel D. I., Bickford M. E. and Orrell S. E. (2000) The use of strontium and lead isotopes to identify sources of water beneath

the Fresh Kills landfill, Staten Island, New York, USA. *Appl. Geochem.* **15**(4), 493–500.

Spiteri C., Regnier P., Slomp C. P. and Charette M. A. (2006) pH-dependent iron oxide precipitation in a subterranean estuary. *J. Geochem. Explor.* **88**, 399–403.

Starinsky A., Bielski M., Lazar B., Wakshal E. and Steinitz G. (1980) Marine Sr-87–Sr88 ratios from the Jurassic to Pleistocene – Evidence from groundwaters in Israel. *Earth Planet. Sci. Lett.* **47**(1), 75–80.

Sultan M., Sturchio N., Al Sefry S., Milewski A., Becker R., Nasr I. and Sagintayev Z. (2008) Geochemical, isotopic, and remote sensing constraints on the origin and evolution of the Rub Al Khali aquifer system, Arabian Peninsula. *J. Hydrol.* **356**, 70–83.

Tripathy G. R. and Singh S. K. (2010) Chemical erosion rates of river basins of the Ganga system in the Himalaya: Reanalysis based on inversion of dissolved major ions, Sr, and $^{87}Sr/^{86}Sr$. *Geochem. Geophys. Geosyst.* **11**, Q03013. http://dx.doi.org/10.1029/2009GC002862.

Uddin A. and Lundberg N. (1998) Cenozoic history of the Himalayan–Bengal system: Sand composition in the Bengal Basin, Bangladesh. *Geol. Soc. Am. Bull.* **110**, 497–511.

van Beek, L. P. H. and Bierkens, M. F. P. (2008) The Global Hydrological Model PCR-GLOBWB: Conceptualization, parameterization and verification, Report Department of Physical Geography, Utrecht University, Utrecht, The Netherlands. <http://vanbeek.geo.uu.nl/suppinfo/vanbeekbierkens2009.pdf>.

Veizer J. (1989) Strontium isotopes in seawater through time. *Ann. Rev. Earth Planet. Sci.* **17**, 141–167.

Vengosh A., Spivack A. J., Artzi Y. and Ayalon A. (1999) Boron, strontium, and oxygen isotopic and geochemical constraints for the origin of salinity in groundwater from the Mediterranean coast of Israel. *Water Resour. Res.* **35**(6), 1877–1894.

Vengosh A., Gill J., Davisson M. L. and Hudson G. B. (2002) A multi-isotope (B, Sr, O, H, and C) and age dating (3H–3He and 14C) study of groundwater from Salinas Valley, California: Hydrochemistry, dynamics, and contamination processes. *Water Resour. Res.* **38**(1), 1008. http://dx.doi.org/10.1029/2001WR000517.

Vengosh A., Marei A., Kloppmann W., Livshitz Y. and Guerrot C. (2005) Tracing the origin of boron and salinity in the Gaza Strip: Natural contaminant transboundary flow in the Mediterranean Coastal Aquifer. *Water Resour. Res.* **41**, W01013. http://dx.doi.org/10.1029/2004WR003344.

Vengosh A., Hening S., Ganor J., Mayer B., Weyhenmeyer C. E., Thomas D., Bullen T. D. and Paytan A. (2007) New isotopic evidence for the origin of groundwater from the Nubian Sandstone Aquifer in the Negev, Israel. *Appl. Geochem.* **22**, 1052–1072.

Vilomet J. D., Angeletti B., Moustier S., Ambrosi J. P., Wiesner M., Bottero J. Y. and Chatelet-Snidaro L. (2001) Application of strontium isotopes for tracing landfill leachate plumes in groundwater. *Environ. Sci. Technol.* **35**(23), 4675–4679.

Widory D., Kloppmann W., Chery L., Bonnin J., Rochdi H. and Guinamant J. L. (2004) Nitrate in groundwater: An isotopic multi-tracer approach. *J. Contam. Hydrol.* **72**(1–4), 165–188.

Wiegand B., Dietzel M., Bielert U., Groth P. and Hansen B. T. (2002) $^{87}Sr/^{86}Sr$-Verhältnisse als Tracer für geochemische Prozesse in einem Lockergesteinsaquifer (Liebenau, NW-Deutschland). *Acta Hydrochim. Hydrobiol.* **29**(2–3), 139–152. http://dx.doi.org/10.1002/1521-401X(200109)29:2/3 (in German).

Windom H. L., Moore W. S., Niencheski L. F. H. and Jahnke R. A. (2006) Submarine groundwater discharge: A large, previously unrecognized source of dissolved iron to the South Atlantic Ocean. *Mar. Chem.* **102**, 252–266.

Woods T. L., Fullagar P. D., Spruill R. K. and Sutton L. C. (2000) Strontium isotopes and major elements as tracers of ground water evolution: Example from the Upper Castle Hayne Aquifer of North Carolina. *Ground Water* **38**(5), 762–771.

Xin, G. (1993) Strontium isotope study of the Peconic River watershed, Long Island, NY. MS thesis. Stony Brook Univ. 83pp.

Young M. B., Gonneea M. E., Fong D. A., Moore W. S., Herrera-Silveira J. and Paytan A. (2008) Characterizing sources of groundwater to a tropical coastal lagoon in a karstic area using radium isotopes and water chemistry. *Mar. Chem.* **109**, 377–394.

Zektser I. S., Everett L. G. and Dzhamalov R. G. (2006) *Submarine Groundwater*. CRC Press, p. 466.

Associate Editor: Karen Johannesson